AGU ADVANCING EARTH AND SPACE SCIENCES

Water Resources Research

RESEARCH ARTICLE
10.1029/2024WR038647

How Does Assimilating SMAP Soil Moisture Improve Characterization of the Terrestrial Water Cycle in an Integrated Land Surface-Subsurface Model?

Haojin Zhao[1,2,3], Carsten Montzka[1], Johannes Keller[1,2], Fang Li[1,2,3], Harry Vereecken[1,2], and Harrie-Jan Hendricks Franssen[1,2]

[1]Agrosphere Institute (IBG-3), Forschungszentrum Jülich, Jülich, Germany, [2]Centre for High-Performance Scientific Computing in Terrestrial Systems: HPSC TerrSys, Forschungszentrum Jülich GmbH, Jülich, Germany, [3]Faculty of Georesources and Materials Engineering, RWTH Aachen University, Aachen, Germany

Key Points:

- Assimilating Soil Moisture Active Passive (SMAP) data improved soil moisture characterization in both models, with the coupled model better capturing spatial variability
- Assimilation showed minimal improvement for ET characterization and did not enhance groundwater level predictions due to system complexities
- Joint state-parameter estimation does not give better estimates than state updating alone as SMAP lack enough information on parameters

Correspondence to:
H. Zhao,
h.zhao@fz-juelich.de

Citation:
Zhao, H., Montzka, C., Keller, J., Li, F., Vereecken, H., & Hendricks Franssen, H.-J. (2025). How does assimilating SMAP soil moisture improve characterization of the terrestrial water cycle in an integrated land surface-subsurface model? *Water Resources Research*, *61*, e2024WR038647. https://doi.org/10.1029/2024WR038647

Received 11 AUG 2024
Accepted 30 MAR 2025

Author Contributions:

Conceptualization: Haojin Zhao, Harry Vereecken, Harrie-Jan Hendricks Franssen
Formal analysis: Haojin Zhao
Methodology: Haojin Zhao
Software: Haojin Zhao, Johannes Keller
Supervision: Carsten Montzka, Harry Vereecken, Harrie-Jan Hendricks Franssen
Validation: Haojin Zhao
Visualization: Haojin Zhao
Writing – original draft: Haojin Zhao
Writing – review & editing: Haojin Zhao, Carsten Montzka, Johannes Keller, Fang Li, Harry Vereecken, Harrie-Jan Hendricks Franssen

Abstract Land surface modeling combined with data assimilation can yield highly accurate soil moisture estimates on regional and global scales. However, most land surface models often neglect lateral surface and subsurface flows, which are crucial for water redistribution and soil moisture. This study applies the Community Land Model (CLM) and the coupled CLM-ParFlow model over a 22,500 km^2 area in western Germany. Soil moisture retrievals from the Soil Moisture Active Passive mission are assimilated with the Localized Ensemble Kalman Filter (with and without parameter estimation). The simulated soil moisture, evapotranspiration (ET) and groundwater level are evaluated using in situ observations from a Cosmic-Ray Neutron Sensor network, Eddy Covariance (EC) stations and groundwater measurement wells. The assimilation improves the median correlation between simulated and measured soil moisture from 0.72 ~ 0.79 to 0.79 ~ 0.83 and decreases the median unbiased Root Mean Square Error (ubRMSE) from 0.063 ~ 0.060 cm^3/cm^3 to 0.050 ~ 0.045 cm^3/cm^3. ET characterization shows a limited improvement with a highest ubRMSE reduction of 15% at the Rollesbroich1 site with the CLM-ParFlow model. The assimilation does not improve the groundwater level characterization. Furthermore, the joint state-parameter update does not outperform state-only update. Overall, the simulation of full 3D subsurface hydrology with the ParFlow model component results in additional model outputs like groundwater levels and river stages, and a better soil moisture characterization (compared to CLM stand-alone), but it does not make soil moisture assimilation more efficient to correct model states.

1. Introduction

Soil moisture impacts crop yield, controls the division of precipitation into surface runoff and soil infiltration, and regulates sensible and latent heat fluxes (Babaeian et al., 2019; Seneviratne et al., 2010). Accurate and large-scale soil moisture data are essential for understanding hydrological processes, predicting weather and extreme events, and developing effective water resources management strategies. While in situ measurement networks, such as Terrestrial Environmental Observatories (TERENO) (Zacharias et al., 2011) in Germany, Texas Soil Observation Network (TxSON) (Clewley et al., 2017) in the USA, and the Tibetan Plateau Observatory of Plateau Scale Soil Moisture and Soil Temperature (Tibet-Obs) (Su et al., 2011) in China, provide high-quality soil moisture observations, their spatial coverage remains limited to specific regions.

Soil moisture can be simulated using land surface models (LSMs), for example, the Community Land Model (CLM) (Oleson et al., 2008) with different spatial and temporal resolutions depending on the research question and the available computational resources. Nevertheless, the accuracy of model predictions is often compromised by uncertainties related to input data. For instance, offline LSMs must be driven by meteorological forcing data sets and are sensitive to the accuracy of the atmosphere forcings (Albergel et al., 2018). In addition, the uncertainties in soil and vegetation properties and model structure errors greatly influence the simulations (Bastidas et al., 2003; Hartley et al., 2017; J. Li et al., 2018; Laguë et al., 2019).

Alternatively, remote sensing techniques provide a possibility to obtain continuous and global soil moisture data. Soil moisture data from satellites like SMOS (Soil Moisture Ocean Salinity) (Kerr et al., 2010) and SMAP (Soil Moisture Active Passive) (Entekhabi et al., 2010) provide exhaustive information at a coarse resolution of 36 km or 9 km, respectively. These satellites capture soil moisture information from the upper soil layer (approximately 5 cm depth), and their accuracy may be influenced by factors such as vegetation type and distribution (Jha

et al., 2007; Konings et al., 2017; Zheng et al., 2018). Data assimilation, a technique that combines observations with model predictions, offers a promising approach to enhance the accuracy of LSMs. Sequential data assimilation in combination with LSMs has been used to provide better estimates for soil moisture for two decades (Han et al., 2014; Koster et al., 2018; Lievens, Martens, et al., 2017; Lievens, Reichle, et al., 2017; Nair & Indu, 2019; Nie et al., 2022; Pleim & Xiu, 2003; Reichle, 2008; Reichle et al., 2002; Yang et al., 2016; Yin et al., 2015).

Several studies have assimilated remotely sensed soil moisture observations into LSMs for the improvement of predictions of soil moisture and other hydrological variables. For example, SMOS and SMAP products have been assimilated into LSMs (e.g., GEOS-5, VIC-CMEM coupled model) with Ensemble Kalman Filter (EnKF) and pronounced improvements in soil moisture characterization are observed (Ahmad et al., 2022; De Lannoy & Reichle, 2016; Lievens et al., 2016; Lievens, Martens, et al., 2017; Reichle et al., 2017). Studies using other satellite-based products (e.g., ESACCI and ASCAT) also demonstrated the potential of assimilating remotely sensed soil moisture information to improve soil moisture estimates (Nair & Indu, 2019; Naz et al., 2019; Pinnington et al., 2018; Zhou et al., 2022). In general, most studies indicate that while the assimilation of remotely sensed retrievals improves soil moisture estimates, the improvement is limited when it comes to characterizing land surface fluxes and estimating runoff (Ahmad et al., 2022; De Santis et al., 2021; Lu et al., 2020; Martens et al., 2016; Naz et al., 2019; Prakash & Mishra, 2023). Traditional LSMs usually do not take into account lateral water exchange, restricting water flow to the vertical direction only. Several studies suggest that groundwater dynamics need to be considered when dealing with land surface processes (Kollet & Maxwell, 2008; Liang et al., 2003; Maxwell & Miller, 2005). A more detailed representation could not only improve soil moisture characterization (Kim & Mohanty, 2017), but also influence energy flux partitioning (Maxwell & Condon, 2016; Z. Zhang et al., 2021), runoff, and groundwater recharge (Holtzman et al., 2020; Wang et al., 2020). Therefore, coupled simulation platforms have been developed to examine the coupled water and energy cycles in the atmosphere-land surface-subsurface continuum (Maxwell et al., 2007; Rummler et al., 2019; Sulis et al., 2017; W. Tian et al., 2012). Such models include Flux with Penn State Integrated Hydrologic Model (PIHM) (Shi et al., 2013), CLM 4.0 with process-based Adaptive Watershed Simulator (Shen et al., 2013), CATchment HYdrology with Noah-Multiparameterization LSM (Noah-MP) (Niu, Paniconi, et al., 2014; Niu, Troch, et al., 2014). Furthermore, the Terrestrial System Modeling Platform (TSMP) (Shrestha et al., 2014) was developed, consisting of three different models which are two-way coupled: the atmospheric simulation model COSMO (Consortium for Small-Scale Modeling) (Baldauf et al., 2011), the LSM CLM 3.5 (the CLM) (Oleson et al., 2008) and the sub-surface hydrological model ParFlow (Kollet & Maxwell, 2006). TSMP can model the water and energy cycles from the very deep subsurface to the stratosphere (Sulis et al., 2017) and is one of the few available modeling platforms that fully integrates the atmospheric, land surface, and subsurface physical processes. TSMP calculates three-dimensional flow over the entire domain and has a detailed physical modeling of the land surface fluxes (Koch et al., 2016). Despite improved representation of LSM processes, a limited number of synthetic studies have investigated the value of data assimilation when employed in conjunction with integrated land surface-subsurface models. These studies (Hung et al., 2022; S. V. Kumar et al., 2009; F. Li et al., 2024; Sawada, 2020) have demonstrated that the information of soil moisture observations can be propagated to the neighboring grid cells and in the vertical profile.

The objective of this study is to conduct, for the first time, an evaluation of assimilating remote sensing soil moisture information into the two-way coupled CLM-ParFlow model within the TSMP framework in a real-world case study. By integrating SMAP data into a high-resolution modeling system that is capable of simulating three-dimensional saturated and unsaturated groundwater flow, it allows us to examine SMAP's potential to improve soil moisture, evapotranspiration and groundwater level characterization compared to traditional LSMs, such as CLM. While SMAP observations are limited to the top 5 cm of soil, where soil moisture dynamics are primarily influenced by vertical fluxes (e.g., infiltration and evaporation), lateral flow processes can indirectly affect surface soil moisture through subsurface moisture redistribution, particularly in regions with complex topography. We evaluate the soil moisture estimates and other predicted variables in both CLM and CLM-ParFlow in situ measurements over a temperate region in western Germany. This paper addresses the following research questions:

1. Does the SMAP soil moisture product provide effective information to improve the characterization of soil moisture states in the high-resolution coupled land surface-subsurface CLM-ParFlow model more than in the stand-alone CLM model?

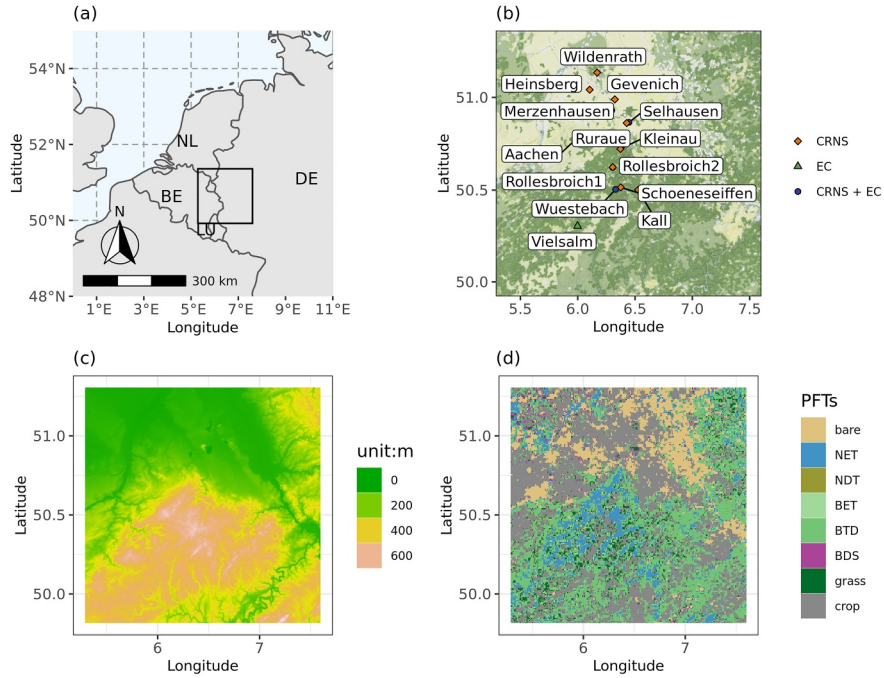

Figure 1. (a) Location of the study area in Europe (DE = Germany; NL = Netherlands; BE = Belgium, LU = Luxemburg); (b) In situ stations for soil moisture (Cosmic-Ray Neutron Sensor) and evapotranspiration (EC) in the study area; (c) Elevation of the region (m, d) The spatial distribution of plant functional types, including bare, needleleaf evergreen tree (NET), needleleaf deciduous tree, broadleaf evergreen tree (NET), broadleaf deciduous tree, broadleaf deciduous shrub, grass and crop.

2. How does assimilating remotely sensed soil moisture affect the characterization of ET in CLM-ParFlow and can the characterization of ET be improved more than for the stand-alone CLM model?
3. How does soil moisture assimilation affect shallow and deep groundwater level predictions in the coupled land surface-subsurface model?
4. Does updating the model parameters, in addition to the states, further improve the simulation of hydrological variables?

2. Materials and Methods

2.1. Study Area and In Situ Data

In this work, SMAP soil moisture data is assimilated into the TSMP model for the so-called NRW-domain, which consists of parts of the North Rhine-Westphalia, Rhineland-Palatinate and Hesse Federal states in western Germany, and includes also parts of Belgium, the Netherlands and Luxemburg (Figure 1). The domain size is 150 km × 150 km. The elevation ranges from 13 m in the northwestern part to 735 m in the southern part. This elevation gradient also influences the precipitation patterns, with the southern region receiving high precipitation amounts reaching up to 1,600 mm annually, whereas the average yearly precipitation in the rest of the research area ranges from 600 to 900 mm (Quirmbach et al., 2012; Zhao et al., 2021). The research area is distinguished by a temperate climate, with average monthly temperatures varying between 3°C in January and 18°C in July in the lower parts of the study domain. It is notable for a high population density and extensive urban development, while the remaining land cover is predominantly composed of grasslands, agricultural fields, and forested regions. TSMP runs over the NRW domain have already been performed by Sulis et al. (2018) and Uebel and Bott (2018).

Cosmic Ray Neutron Sensors (CRNS) measurements are an emerging technology for monitoring soil moisture at the intermediate scale. The measurement radius ranges between 130 and 300 m as function of factors like air density, air humidity and vegetation density (Köhli et al., 2015; Zreda et al., 2012). The penetration depth of CRNS measurements varies from 15 cm (wet soils) to 80 cm (dry soils) (Franz et al., 2012; Köhli et al., 2015). Several studies have been conducted to investigate the accuracy of the CRNS measurements (Jakobi et al., 2018;

Table 1
Cosmic-Ray Neutron Sensor and EC Stations: Coordinates, Altitude From Digital Elevation Model (DEM) (m), Average Annual Precipitation (mm y^{-1}), Plant Functional Types and Soil Texture Information (H. R. Bogena et al. (2022), Baatz et al. (2017)

Name	Latitude	Longitude	DEM	Precip.	Plant functional type	Clay %	Sand %
Merzenhausen	50.930	6.297	91	718	Crop	22	21
Aachen	50.799	6.025	232	865	Crop	23	22
Selhausen	50.866	6.447	101	718	Crop	24	16
Heinsberg	51.041	6.104	58	722	Grassland, crop	19	18
Wüstebach	50.505	6.331	607	1180	Forest	23	19
Gevenich	50.989	6.324	107	718	Crop	20	22
Rollesbroich1	50.622	6.304	515	1018	Grassland	23	22
Rollesbroich2	50.624	6.305	506	1018	Grassland	–	–
Ruraue	50.862	6.427	100	718	Grassland	26	19
Wildenrath	51.133	6.169	72	722	Forest	12	65
Kall	50.501	6.526	505	857	Grassland	22	20
Schoeneseiffen	50.515	6.376	611	870	Grassland	24	16
Kleinau	50.722	6.372	374	614	Grassland	25	15
Vielsam	50.305	5.998	493	1062	Forest	–	–

Z. Tian et al., 2016; Zhu et al., 2016). In the study by H. Bogena et al. (2013), it is found that the root mean square error (RMSE) of daily soil moisture data was about 0.03 cm^3/cm^3 for the forested site Wüstebach in Germany, which has in general very high soil moisture content. Thirteen CRNS stations are located in the research domain and are used for the verification of the simulations and data assimilation experiments. Table 1 provides further details. The penetration depth z^* of the CRNS measurements is calculated and given by Franz et al. (2012):

$$z^* = \frac{5.8}{\theta + 0.0829} \tag{1}$$

where θ is the total soil water content. In order to compare measured soil moisture content by CRNS with simulated soil moisture content, the soil moisture contents simulated for the different layers at different depths d have to be weighted. The weights W_d are determined based on the following relation:

$$W_d = \begin{cases} 1 - d/z^*, & d \le z^* \\ 0, & d > z^* \end{cases} \tag{2}$$

A weighted average of soil moisture θ_{z^*} is calculated over L vertical layers with depths d_i, simulated soil moisture θ_{d_i} and weights W_{d_i}:

$$\theta_{z^*} = \frac{\sum_{i=1}^{L} W_{d_i} \cdot \theta_{d_i}}{\sum_{i=1}^{L} W_{d_i}} \tag{3}$$

The eddy covariance (EC) method allows to measure ET at the field scale. Four eddy covariance sites are located in our study domain and are part of the FLUXNET2015 data set (Pastorello et al., 2020), including Selhausen (crop land), Rollesbroich (grassland), Wüstebach (forest), and Vielsam (forest). Raw data, including fluxes of latent heat, sensible heat, CO_2 and meteorological variables, at high frequencies (10–20 Hz) and can be processed into coarser time steps, such as half-hourly or daily resolutions at each site (Pastorello et al., 2020). The data gaps in fluxes and meteorological time series are filled, undergo quality checks, and are aggregated to daily observations (Ukkola et al., 2017). Figure 1 shows the spatial locations of the CRNS and EC stations.

The groundwater level observations are obtained from the monitoring network Geoportal NRW (https://www.geoportal.nrw) and Groundwatertools (https://www.grondwatertools.nl). A total of 977 groundwater wells are available in this research area, providing monthly observations throughout the year 2018. Of these, only 527 wells with shallow groundwater levels (less than 30 m deep) are included in the analysis.

2.2. SMAP (L3_SM_P_E) Product

SMAP provides soil moisture measurements of approximately the top 5 cm of the soil and thaw/freeze state that can be used in hydrological models and LSMs. The SMAP satellite completes a global soil moisture map with a repetition of 2 ∼ 3 days and its orbit is exactly 8 days (P. E. O'Neill et al., 2021). Compared to other L-band sensors, for example, SMOS, the assimilation of SMAP data shows higher skill (Blyverket et al., 2019; L. Zhang, Kim, & Sharma, 2019).

In this study, the L3_SM_P_E product from National Snow and Ice Data Center NSIDC (https://nsidc.org/data/smap/smap-data.html) is used, which provides soil moisture on a 9 km grid for the upper 5 cm soil with an error of no greater than 0.04 cm^3/cm^3 (Colliander et al., 2017). The SMAP Enhanced Passive Soil Moisture Products (L2_SM_P_E and L3_SM_P_E) have been developed after the SMAP radar stopped operation in July 2015. To enhance the resolution of SMAP radiometer data, the Backus-Gilbert optimal interpolation technique is used to make most use of the additional information and provide a better representation of the original data (Chan et al., 2017). L3_SM_P_E is a daily composite product that is generated from L2_SM_P_E over one day composition. This enhanced product was assessed by comparing it with long-term in situ soil moisture data and it was found that the average unbiased Root Mean Square Error (ubRMSE) of the level 3 product is around 0.045 ∼ 0.055 cm^3/cm^3 (Chan et al., 2017; Colliander et al., 2021; Montzka et al., 2017; L. Zhang, Kim, & Sharma, 2019; R. Zhang, Kim, & Sharma, 2019).

2.3. CLM - ParFlow in TSMP

The Terrestrial Systems Modeling Platform (TSMP) consists of the atmospheric model COSMO (Baldauf et al., 2011), the LSM CLM 3.5 (Oleson et al., 2008) and the subsurface model ParFlow (Kollet & Maxwell, 2006). These models are two-way coupled by the Ocean Atmosphere Sea Ice Soil Model Coupling Toolkit, OASIS-MCT (Valcke, 2013). COSMO is the operational weather forecast model of the German weather service (Baldauf et al., 2011). TSMP provides a flexible coupling arrangement that enables fully coupled simulations (COSMO + CLM + ParFlow) as well as partially coupled simulations (COSMO + CLM or CLM + ParFlow). Additionally, each of the three models can be run independently. When simulating CLM or CLM coupled with ParFlow, external forcing data is necessary to provide the required boundary conditions.

2.3.1. The Land Surface Model - CLM

CLM 3.5 models the water and energy cycles in the soil-vegetation-atmosphere continuum including snow packs. Five land cover types are defined in this model to characterize surface heterogeneity, including glacier, lake, wetland, urban and vegetated. Snow accumulation is represented with up to five snow layers on top of the soil layers. Plant properties are assigned on the basis of different plant functional types (PFTs). CLM has 10 soil layers with varying thicknesses. Runoff calculation in CLM is based on the traditional TOPMODEL (Oleson et al., 2004) approach. Hydraulic conductivity and porosity are determined by soil texture (% sand and % clay) based on pedotransfer functions (Clapp & Hornberger, 1978; Cosby et al., 1984). A simplified Richards equation is used to calculate the water movement in the unsaturated zone:

$$\frac{\partial \theta}{\partial t} = \frac{\partial}{\partial z}\left[k\left(\frac{\partial \theta}{\partial z}\frac{\partial \psi}{\partial t}\right) + 1\right] \tag{4}$$

where θ represents the volumetric soil water content [L^3/L^3], t is time [T], k is the hydraulic conductivity [L/T], z is height [L] and ψ is pressure head [L].

The hydraulic conductivity between two adjacent layers $k_{i,j}$ can be calculated as:

$$k_{i,j} = \begin{cases} k_{s(i,j)} \left[\dfrac{0.5(\theta_{liq,j}) + 0.5(\theta_{liq,j+1})}{0.5(\theta_{sat,j}) + 0.5(\theta_{sat,j+1})} \right]^{2B_j+3}, & 1 \le j \le 9 \\ k_{s(i,j)} \left[\dfrac{\theta_{liq,j}}{\theta_{sat,j}} \right]^{2B_j+3}, & j = 10 \end{cases} \quad (5)$$

and i and j are layer indices. θ_{liq} is the volumetric liquid water content and θ_{sat} is the soil moisture content at saturated state. The saturated hydraulic conductivity $k_{s(i,j)}$ is assumed to be exponentially decreasing with depth following the TOPMODEL concept (Beven & Kirkby, 1979):

$$k_{s(i,\,j)} = 0.0070556 \times 10^{-0.884+0.0153(\%sand)_j)} \left[\exp\left(-\frac{z_{i,j}}{z_0} \right) \right] \quad (6)$$

where $z_0 = 0.5$ m is the length scale for decrease in $k_{s(i,\,j)}$, $z_{i,\,j}$ represents height at the interface between i and j, and the exponent B_j is calculated as:

$$B_j = 2.91 + 0.159(\%clay)_j \quad (7)$$

The saturated water content θ_{sat} (i.e., porosity ϕ) is calculated as:

$$\theta_{sat} = 0.489 - 0.00126(\%sand) \quad (8)$$

In the CLM model, the mass transfer equation (MT) and Monin-Obukhov Similarity Theory are used to calculate evapotranspiration (ET). The ground evaporation, evaporation from interception and transpiration are separately considered. For the vegetated areas, the water vapor flux from vegetation E_v [M/L^2/T] and from ground soil E_g [M/L^2/T] are calculated as follows:

$$E_v = -\rho_{atm} \frac{(q_s - q_{sat}^{T_v})}{r_{total}} \quad (9)$$

$$E_g = -\rho_{atm} \frac{(q_s - q_g)}{r_{aw}{}'} \quad (10)$$

where ρ_{atm} is the atmospheric air density [M/L^3], q_s is the canopy specific humidity [M/M], $q_{sat}^{T_v}$ is the saturated specific humidity [M/M] at the vegetation temperature T_v, r_{total} [T/L] is the total resistance to water vapor transfer from the canopy to the canopy air, caused by both the leaf boundary layer and stomatal resistance, q_g is the specific humidity of ground, and $r_{aw}{}'$ is the aerodynamic resistance [T/L] to water vapor transfer, from the ground to the canopy air. A detailed description of the soil moisture content and ET calculation process can be found in the CLM technical description document (Oleson et al., 2004).

2.3.2. The Subsurface Model - ParFlow

ParFlow is a numerical, integrated hydrological model that simulates subsurface flow in unsaturated and saturated porous media, as well as overland flow. ParFlow solves the pressure in the subsurface and interactions with surface water bodies. The saturated-unsaturated subsurface flow equation is solved in three dimensions according to Richards. The surface water routing scheme is based on the kinematic wave approximation of overland flow, while coupling subsurface flow and overland flow in an integrated fashion (Kollet & Maxwell, 2006). Both the soil water retention curve and relative permeability are represented in ParFlow using the van Genuchten relationships (Maxwell & Miller, 2005). The water retention curve and relative permeability in the Van Genuchten model are defined as follows:

$$\theta_\psi = \theta_{sat} + \frac{\theta_{sat} - \theta_{res}}{[1 + (\alpha \cdot \psi)^n)]^{1-1/n}} \quad (11)$$

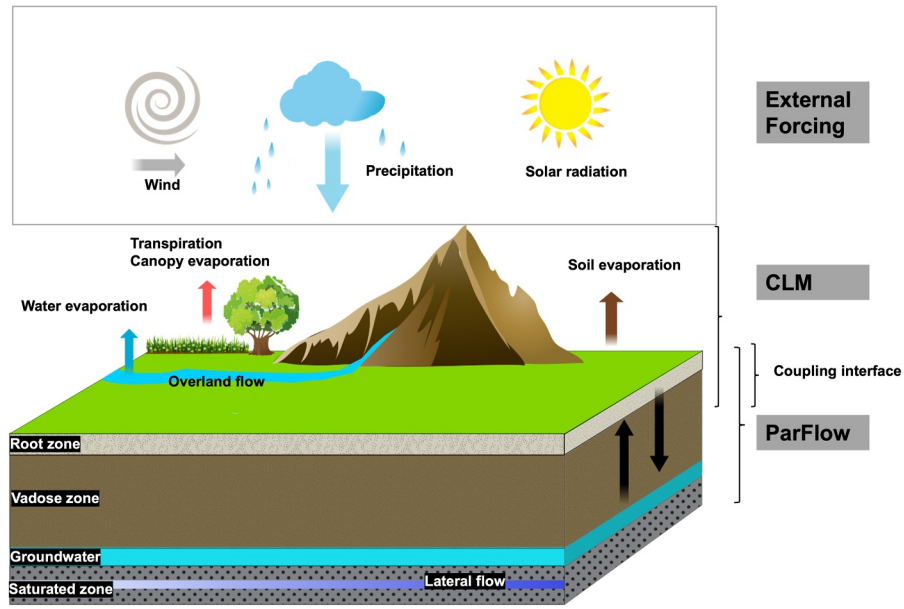

Figure 2. Schematic diagram of CLM-ParFlow in TSMP.

$$k_r = \frac{\left[1 - \frac{(\alpha \cdot \psi)^{n-1}}{(1+(\alpha \cdot \psi)^n)^{1-1/n}}\right]^2}{(1+(\alpha \cdot \psi)^n)^{(1-1/n)/2}} \tag{12}$$

Where ψ is the suction pressure [L] and k_r is the relative permeability [−]. α ($\alpha > 0$) [L^{-1}] and n ($n > 1$) are soil parameters that are related to air entry suction for drying/wetting and slopes in van Genuchten curves. θ_{sat} and θ_{res} represent saturated water content and residual water content respectively (L^3/L^3). More details of this model can be found in Kollet and Maxwell (2006, 2013).

2.3.3. The Integrated CLM-ParFlow

The coupled CLM-ParFlow model is used in this work. A schematic representation of CLM-ParFlow in TSMP is shown in Figure 2. The offline atmospheric forcing drives the CLM to model land surface processes. ParFlow replaces the one-dimensional soil hydrology of CLM with a three-dimensional approach. The models are coupled via net infiltration (CLM calculates net infiltrating water for ParFlow), soil evaporation and transpiration (including root water uptake) (CLM calculates water to be extracted by ParFlow), and ParFlow provides CLM with saturation and pressure for the top 10 layers simultaneously (Shrestha et al., 2014).

2.4. Data Assimilation

The data assimilation framework PDAF (Nerger et al., 2005; Nerger & Hiller, 2013) has already been coupled to TSMP (Kurtz et al., 2016). TSMP-PDAF includes data assimilation algorithms like the EnKF (Evensen, 1994) and its variants, for example, the localized Ensemble Kalman Filter (LEnKF) (Ott et al., 2004) and the local ensemble transform Kalman filter (Hunt et al., 2007). In this study, the EnKF is used to assimilate SMAP soil moisture data into TSMP. EnKF has already been proven to be robust and computationally efficient, suitable for large-scale non-linear models (Zamani et al., 2010).

2.4.1. Ensemble Kalman Filter

The first step in the EnKF is the forecast step, where the model $\mathbf{M}$ calculates the state $\mathbf{x}^t$ at time t:

$$\mathbf{x}^t = \mathbf{M}\left(\mathbf{x}^{t-1}, \mathbf{p}, \mathbf{q}\right)^t \tag{13}$$

where $\mathbf{p}$ is the vector with parameters and $\mathbf{q}$ is the vector with model forcings. This forecast step is carried out N times, for each of the ensemble members j. The different ensemble members can have different atmospheric forcings, model parameters and initial conditions, which should adequately capture the uncertainty in these variables. The observation equation is:

$$\mathbf{y}^t = \theta^t + \boldsymbol{\varepsilon}^t \tag{14}$$

where $\mathbf{y}^t$ is the vector with measurements at the current time step t. In this study, the soil moisture observations θ are assimilated. $\boldsymbol{\varepsilon}^t$ is a random vector containing the measurement errors. The model states for each of the realizations are updated to $\mathbf{x}^{t,a}$ by combining forecasts and the observations $\mathbf{y}^t$:

$$\mathbf{x}^{t,a} = \mathbf{x}^t + \mathbf{K}\left(\mathbf{y}^t - \mathbf{H}\mathbf{x}^t\right) \tag{15}$$

where $\mathbf{H}$ is the operator that links measurements and model states, and the Kalman gain $\mathbf{K}$ is defined as follows:

$$\mathbf{K} = \mathbf{C}^f\mathbf{H}^\mathbf{T}\left(\mathbf{H}\mathbf{C}^f\mathbf{H}^\mathbf{T} + \mathbf{R}\right)^{-1} \tag{16}$$

where $\mathbf{C}$ is the covariance matrix of the model states and $\mathbf{R}$ is the measurement error-covariance matrix. We calculate $\mathbf{C}$ by:

$$\mathbf{C}^f = \frac{1}{N-1}\sum_{j=1}^{N}\left(\mathbf{x}_i^t - \bar{\mathbf{x}}^t\right)\left(\mathbf{x}_j^t - \bar{\mathbf{x}}^t\right) \tag{17}$$

where $\bar{\mathbf{x}}^t$ represents the matrix with the ensemble mean of the model states at time t. N is the number of ensemble members.

In some cases, the model parameters $\mathbf{p}$ are estimated together with the state variables by augmenting the vector $\mathbf{x}$ (Hendricks Franssen & Kinzelbach, 2008). The augmented state vector for updating both states and parameters is given by:

$$\mathbf{x}^{t*} = \begin{pmatrix}\mathbf{x}^t \\ \mathbf{p}^t\end{pmatrix} \tag{18}$$

The model covariance matrix $\mathbf{C}$ is then also composed of the cross covariances between the model states and the model parameters, as well as the covariances among the parameters.

$$\mathbf{C}^f = \begin{pmatrix}\mathbf{C}_{\mathbf{xx}} & \mathbf{C}_{\mathbf{xp}} \\ \mathbf{C}_{\mathbf{px}} & \mathbf{C}_{\mathbf{pp}}\end{pmatrix} \tag{19}$$

2.4.2. Localization

In the EnKF data assimilation, localization reduces the size of the matrix to be inverted to minimize the influence of distant observations and removing spurious long-distance correlations (Houtekamer & Mitchell, 1998). In the localization process, the calculation of the model covariance matrix $\mathbf{C}$ is replaced by $\boldsymbol{\rho}\circ\mathbf{C}$. $\boldsymbol{\rho}$ is defined as a correlation matrix with local support, which means that this function is only non-zero in a local (small) region and zero elsewhere. $\circ$ is the Schur (elementwise) product. Note that $\boldsymbol{\rho}$ and $\mathbf{C}$ have the same dimensions. Therefore, the Kalman gain in the LEnKF scheme is calculated as follows:

$$\mathbf{K} = \left[\boldsymbol{\rho}\circ\mathbf{C}_j^f\mathbf{H}^\mathbf{T}\right]\left[\boldsymbol{\rho}\circ\mathbf{H}\mathbf{C}^f\mathbf{H}^\mathbf{T} + \mathbf{R}\right]^{-1} \tag{20}$$

and $\boldsymbol{\rho}\circ$ is calculated using a fifth-order polynomial function (Gaspari & Cohn, 1999).

Table 2
Node Depth z, Thickness Δz_1, and Depth at the Layer Interface z_{h1} of the Ten Soil Layers Within the Community Land Model Model, Thickness Δz_2, and Depth of the Layer Interface z_{h2} of the Ten Soil Layers Within the CLM-ParFlow Model

Layer i	z : m	Δz_1 : m	z_{h1}	Δz_1 : m	z_{h2}
1 (top)	0.0071	0.0175	0.0175	0.02	0.02
2	0.0279	0.0276	0.0451	0.03	0.05
3	0.0623	0.0455	0.0906	0.05	0.10
4	0.1189	0.0750	0.1655	0.07	0.17
5	0.2122	0.1236	0.2891	0.13	0.30
6	0.3661	0.2038	0.4929	0.20	0.50
7	0.6198	0.3360	0.8289	0.30	0.80
8	1.0380	0.5539	1.3828	0.50	1.30
9	1.7276	0.9133	2.2961	0.70	2.00
10	2.8646	1.5058	3.8019	1.00	3.00

3. Experimental Setup

3.1. Input Data

The spatial model resolution is 500 m × 500 m in the lateral horizontal direction. The soil depth in the CLM stand-alone model reaches to 2.86 m with 10 near surface layers, and in CLM-ParFlow to 30 m depth, with 10 near surface layers with increasing thicknesses from 0.02 to 1 m and 20 vertical layers with a thickness of 1.35 m each (see Table 2). The input data for CLM consist of topography (Figure 1), PFTs (Figure 1), associated plant physiological parameters and soil properties (Figure 3). The soil texture information is taken from SoilGrids (Hengl et al., 2014, 2017) and remapped to the model grid using the Nearest Neighbor (NN) approach (Boas et al., 2023). The PFTs and Leaf Area Index (LAI) are extracted from the Moderate Resolution Imaging Spectroradiometer (MODIS) product and details can be found in Shrestha et al. (2014).

To keep the consistency between the CLM and CLM-ParFlow models, a Rosetta model (Y. Zhang & Schaap, 2017) is used to estimate the saturated hydraulic conductivity in the surface layers (0–3 m below the surface) of CLM-ParFlow. The Rosetta model takes the soil texture information from CLM. The porosity (ϕ) in the surface layers of CLM-ParFlow is calculated based on the same function that is used in the CLM model. For lower layers (3–30 m), the permeability information was taken from a global geological data set (Gleeson et al., 2011), for details see Shrestha et al. (2014). Other van Genuchten water retention parameters (e.g., α and n) are assigned constant, spatially uniform values that are adopted from previous studies (Shrestha et al., 2014; Sulis et al., 2017). The soil texture in CLM and hydraulic parameters in CLM-ParFlow for the surface layers and bottom layers are shown in (Figure 3). Sandy soils are mainly located in the northwestern corner of the research domain, leading to a high hydraulic conductivity there. An impermeable boundary condition is defined for the lateral borders of the subsurface.

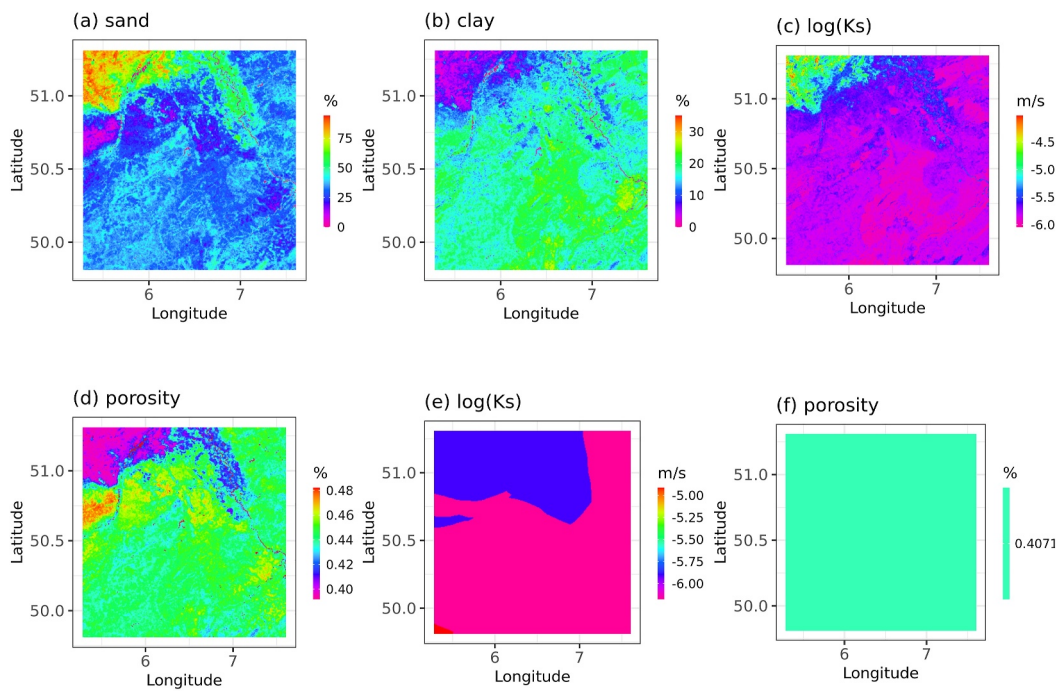

Figure 3. (a, b) Percentages of sand and clay used in the Community Land Model stand-alone model. (c, d) Saturated hydraulic conductivity K_s and porosity for the surface layer (0–3 m depth) in the CLM-ParFlow model. (e, f) show the same for the bottom layer (3–30 m depth).

Table 3
Correlation Matrix of Perturbed Atmospheric Forcing Variables

Variable name	Precipitation	Shortwave radiation	Longwave radiation	Temperature
Precipitation	1	−0.8	0.5	0.0
Shortwave radiation	−0.8	1.0	−0.5	0.4
Longwave radiation	0.5	−0.5	1.0	0.4
Temperature	0.0	0.4	0.4	1.0

Atmospheric forcing is extracted from the high-resolution reanalysis data set COSMO-REA6 (Bollmeyer et al., 2015) and used as input for CLM. COSMO-REA6 was created by assimilating observed meteorological data into the atmospheric model COSMO at 6 km resolution over the European continent. In the COSMO-REA6, ERA-interim data (Dee et al., 2011) are used as lateral boundary conditions. Compared to other data sets, such as ERA-interim (at 80 km resolution) and ERA5 (at 25 km resolution), the COSMO-REA provides a higher resolution atmospheric reanalysis. It is shown that the high-resolution reanalysis provides additional value compared to coarse scale reanalysis and leads to a better representation of small-scale variability (Bollmeyer et al., 2015). A subset of highly requested variables can be directly downloaded from the open data server at DWD (ftp://opendata.dwd.de/climate_environment/REA/COSMO_REA6), including essential variables which were used in this study, for example, wind speed, air humidity, air pressure, air temperature, precipitation, downward short wave radiation and downward long wave radiation.

3.2. Experiment Set Up and Analyses

The localized EnKF scheme is used in the data assimilation experiments with an ensemble of $N = 32$ members. To characterize the uncertainty of the land surface-subsurface simulations, random perturbations are introduced for each ensemble member, including (a) atmospheric forcings for both the CLM stand-alone model and the CLM-ParFlow model, (b) soil texture for the CLM stand-alone model and (c) hydraulic conductivity and porosity for the soil (0–3 m depth) of the CLM-ParFlow model. Four atmospheric variables, including precipitation, air temperature, long-wave radiation and short-wave radiation are perturbed in a spatially and temporally homogeneous manner with correlations among the four variables defined by a correlation matrix (shown in Table 3). The mean value and standard deviation of the perturbation of precipitation, air temperature, long-wave radiation and short-wave radiation are (0, 0 K, 0 W/m^2, 0) and (0.15, 1.5 K, 30 W/m^2, 0.15) respectively. While the noise (lognormally distributed) for precipitation and shortwave radiation perturbations is introduced multiplicatively, the noise for longwave radiation and temperature perturbations is additive. Precipitation is multiplied by log-normally distributed noise and a bias is introduced by the back transformation (Han et al., 2013). Therefore, a constant correction factor (0.95) is applied to each of the ensemble members.

In the CLM stand-alone simulations, soil texture is perturbed by adding a spatially uniform noise to both % sand and % clay (±10%). The sum of sand and clay percentages is constrained to be smaller than 100% for each ensemble member. For CLM-ParFlow experiments, the ensemble of soil texture data used in CLM is transformed into input parameters for CLM-ParFlow in the surface layers. Hydraulic conductivity realizations are generated using the Rosetta model, while porosity realizations are calculated using Equation 8. Consequently, the perturbation of hydraulic conductivity and porosity is also spatially uniform. The hydraulic conductivity and porosity for the bottom aquifer layers are not perturbed.

To initiate model simulations with the CLM stand-alone model, the model is first spun up using atmospheric forcing data from the years 2015–2017. CLM-ParFlow, on the other hand, has a more comprehensive characterization of the terrestrial water cycle and a dynamic equilibrium needs to be reached to have a more proper model initialization (Ajami et al., 2014). It is spun up with initial states from a previous study (Sulis et al., 2017) and then using forcing data of the year 2017 until a dynamic equilibrium is reached. The DA experiments are conducted in the subsequent year 2018.

Soil moisture from SMAP products is quality controlled by internal quality flags. The measurement depth of SMAP is considered to be 5 cm. The localization radius is set to 20 grid cells (10 km) to take into account the approximal size of the Backhus-Gilbert optimal interpolated original SMAP footprints. The measurement error is

Table 4
Summary of the Six Numerical Experiments Conducted in This Study for the Community Land Model and CLM-ParFlow Models, Along With Their Respective Abbreviations Used in the Subsequent Tables and Figures

Model	Scenario	Abbreviation
CLM	Open loop	CLM-OL
	LEnKF with state update	CLM-DA
	LEnKF with state and parameter update	CLM-DA-SP
CLM-ParFlow	Open loop	CLM-PFL-OL
	LEnKF with state update	CLM-PFL-DA
	LEnKF with state and parameter update	CLM-PFL-DA-SP

set to 0.04 cm^3/cm^3 which is the target accuracy of SMAP mission. The assimilation experiments are run with a one-hour time step, while soil moisture data assimilation is performed daily. In previous studies (Zhao et al., 2021), it was demonstrated that there is no systemic bias present between simulated soil moisture by CLM-ParFlow, SMAP soil moisture retrieval and in situ soil mositure measurements, and as such, there is no requirement for bias correction. The CLM model is reported to have an overestimation of soil moisture in a number of studies (Naz et al., 2019; Zhao et al., 2021). Conversely, the SMAP observations exhibit less bias in comparison to in situ measurements. We consider that applying a bias correction (e.g., the cumulative distribution function) matching technique (Reichle & Koster, 2004) is not suitable here. The relative systematic errors between SMAP soil moisture and CLM-modeled soil moisture are not taken into account in this case.

In this study, six simulation experiments (see also Table 4) are conducted using the TSMP-PDAF framework: (a) CLM-OL: an open-loop simulation (without data assimilation) using CLM stand-alone; (b, c) assimilation of SMAP L3_SM_P_E soil moisture into CLM model, employing either state-only update (CLM-DA) or state and parameter update (CLM-DA-SP); (d) CLM-PFL-OL: an open-loop simulation with the CLM-ParFlow; (e, f) CLM-PFL-DA and CLM-PFL-DA-SP, similar to (b, c) but with the CLM-ParFlow model. When updating both states and parameters in the CLM-ParFlow model, a damping factor of 0.1 is employed to limit the intensity of the hydraulic conductivity perturbations (Hung et al., 2022; F. Li et al., 2024).

3.3. Evaluation Metrics

To assess the influence of the assimilation, statistical performance measures were evaluated, including bias, RMSE, ubRMSE, and Pearson's correlation coefficient (r) (Gruber et al., 2020) and a normalized error reduction index (NER):

$$bias = \frac{1}{T}\sum_{i=1}^{T}(X_{t_i} - Y_{t_i,obs}) \tag{21}$$

$$RMSE = \sqrt{\frac{1}{T}\sum_{i=1}^{T}(X_{t_i} - Y_{t_i,obs})^2} \tag{22}$$

$$ubRMSE = \sqrt{RMSE^2 - bias^2} \tag{23}$$

$$r_{X,Y} = \frac{cov(X,Y)}{\sigma_X \sigma_Y} \tag{24}$$

$$NER = 100 \times \left(1 - \frac{E_{DA}}{E_{OL}}\right) \tag{25}$$

where T is the total number of time steps, X_{t_i} is the modeled ensemble mean variable (soil moisture, ET or groundwater level) and $Y_{t_i,obs}$ is the corresponding observed value, both at time step t_i. $cov(X,Y)$ is the covariance between model simulated values and observed values, σ_X is the standard deviation of model simulated values, and

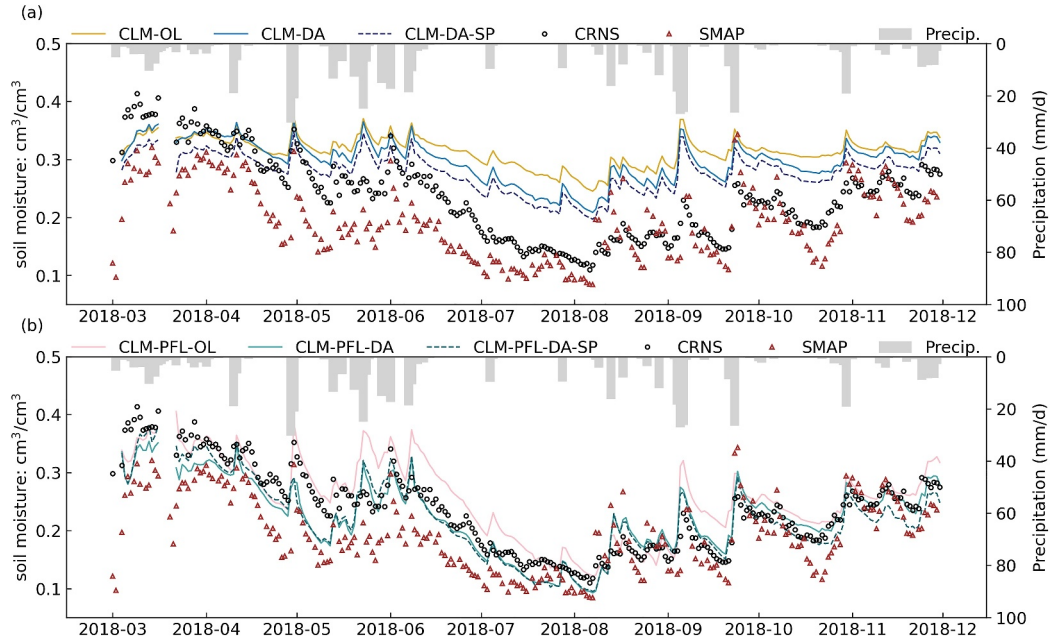

Figure 4. Time series of simulated daily soil moisture (at the depth corresponding to the Cosmic-Ray Neutron Sensor (CRNS)) average over 13 CRNS sites from (a) CLM-OL, CLM-DA and CLM-DA-SP and (b) CLM-PFL-OL, CLM-PFL-DA and CLM-PFL-DA-SP) along with soil moisture measurements by Soil Moisture Active Passive (SMAP) (green triangles) and CRNS (black circles), and precipitation for the simulation period of 2018.03.01–2018.11.30. The CRNS observations are shown in black circles and SMAP observations are shown in green triangles.

σ_Y is the standard deviation of observed values. The E_{DA} and E_{OL} represent the RMSE from the data assimilation and open-loop runs.

4. Results and Discussion

4.1. Evaluation With In Situ Soil Moisture Measurements

Figure 4 compares the soil moisture time series simulated by CLM and CLM-PFL for the OL, DA and DA-SP experiments, with in situ measurements and SMAP observations. Figure 4 shows the seasonal dynamics in both observations and simulated data sets, with the highest soil moisture in early spring and a distinct dry-down from May into the summer time. The simulated soil moisture from CLM-OL is systematically higher than the measurements. Data assimilation corrects the overestimation of soil moisture, especially under drier conditions in the summer season. In general, the simulated soil moisture from CLM-ParFlow shows better temporal consistency with in situ measurements and the SMAP retrievals.

Figure 5 summarizes the evaluation metrics for CLM and CLM-PFL, with and without data assimilation experiments compared with 13 CRNS observations. It shows that both CLM-DA and CLM-DA-SP experiments are closer to in situ soil moisture measurements in terms of ubRMSE and R than the open loop runs. The median ubRMSE decreases from 0.063 cm^3/cm^3 to 0.060 cm^3/cm^3 for CLM-DA and 0.060 cm^3/cm^3 for CLM-DA-SP, meanwhile, the median R increases from 0.72 to 0.79 and 0.78, respectively. For CLM-PFL, the median ubRMSE and R for OL and two DA scenarios are 0.050 cm^3/cm^3, 0.045 cm^3/cm^3 and 0.046 cm^3/cm^3, 0.78, 082 and 0.83 respectively. Overall, compared to the OL runs, assimilation with the CLM and CLM-PFL models lead to small but improved estimates of soil moisture in terms of Pearson r and ubRMSE. It is important to note that while improvements are observed in the median values for Pearson r and ubRMSE, the mean values do not demonstrate a significant improvement for the CLM-ParFlow model. This discrepancy suggests an increased variability in site-specific performance, with some locations exhibiting a deterioration following assimilation. One potential explanation for this is the scale mismatch between the high-resolution model (500 m) and the coarser resolution of the SMAP data (9 km). In the assimilation process, multiple sites are located within the same SMAP grid cell, leading to homogenized updates that may not reflect the finer-scale dynamics captured by CLM-ParFlow.

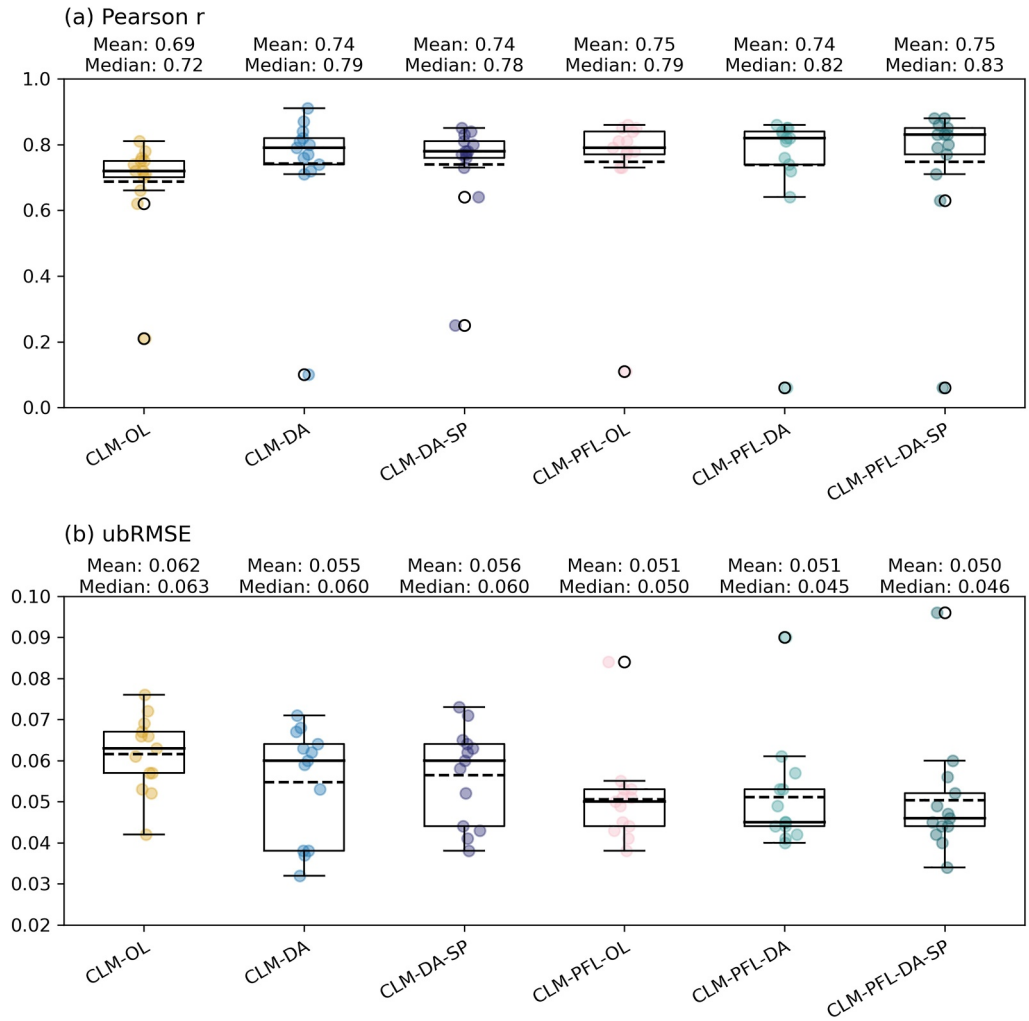

Figure 5. Boxplots of (a) r and (b) unbiased Root Mean Square Error for the simulated soil moisture in the CLM-OL, CLM-DA and CLM-DA-SP and CLM-PFL-OL, CLM-PFL-DA and CLM-PFL-DA-SP simulations compared to Cosmic-Ray Neutron Sensor measurements for the simulation period of 2018.03.01–2018.11.30. The box plot shows the 10%, 25%, 50%, 75%, and 90% quantiles, with the dashed line representing the mean values and circle marks representing the outliers.

The performance of the CLM and CLM-PFL models in simulating soil moisture varies across the 13 site (see Figures A1, A2, and 6). For example, at the Heinsberg and Gevenich sites, the DA runs with CLM and CLM-PFL show the best agreement with the CRNS measurements, with R values above 0.83 and ubRMSE values below 0.041 cm^3/cm^3. At the Merzenhausen site, the performance of the CLM-PFL-DA and CLM-PFL-DA-SP simulations is somewhat lower than CLM-DA and CLM-DA-SP. The assimilation behaves poorly for some stations like Wüstebach, where the ubRMSE of the OL is lower than for the DA runs. The soil in Wüstebach site has high organic matter content, resulting in a high porosity, which is not considered by the pedotransfer functions used for both models. In general, the coupled model CLM-PFL with data assimilation tends to result in the lowest ubRMSE value and highest correlation across most sites. The site-to-site variability can be attributed to the limited footprint of CRNS measurements, which have a radius of approximately 130–300 m. While this footprint is relatively close to the model grid resolution, it only partially covers a model grid cell. This partial overlap introduces additional uncertainty when comparing observed and simulated soil moisture, particularly in regions where soil moisture exhibits high spatial variability. Furthermore, factors such as dense vegetation cover, soil texture, and topographical features are known to impact SMAP observations, thereby affecting their integration into SM simulations.

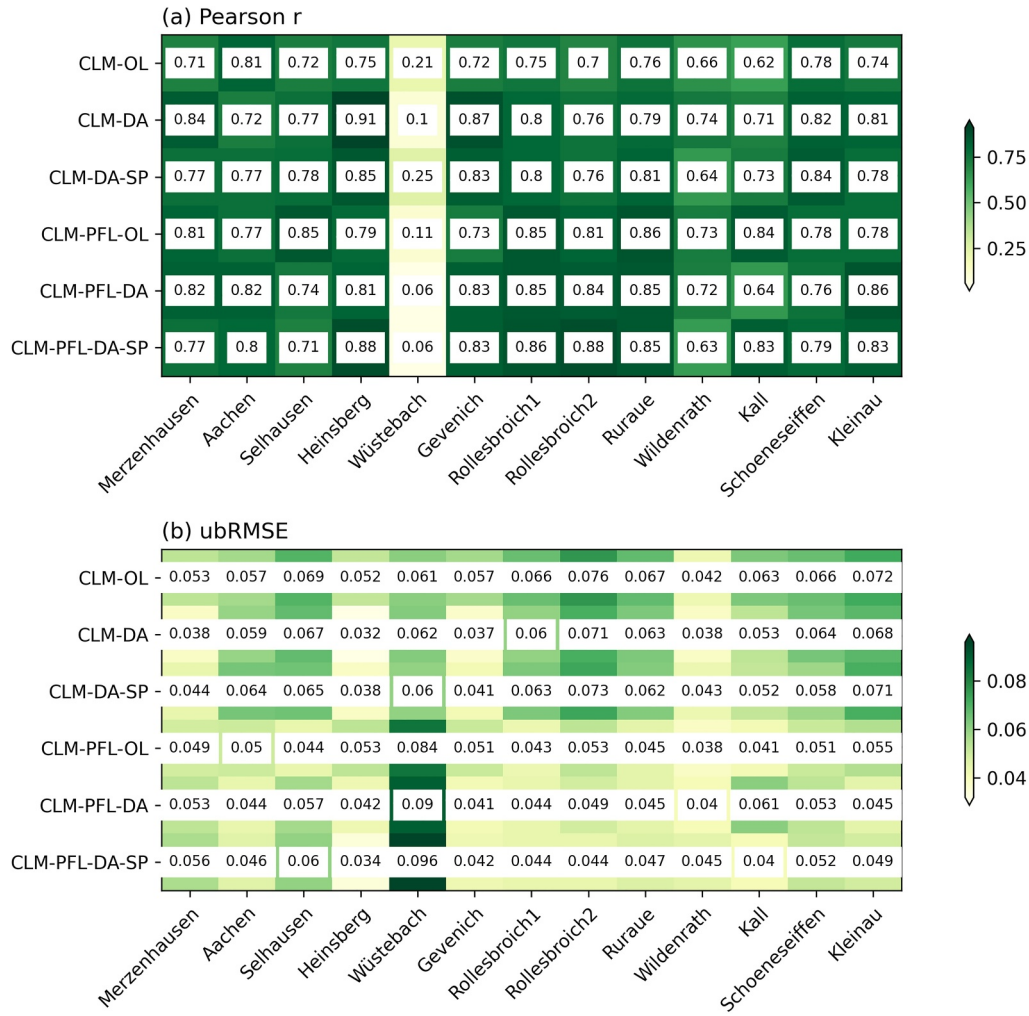

Figure 6. Performance metrics of (a) r and (b) unbiased Root Mean Square Error for the simulated soil moisture in the CLM-OL, CLM-DA and CLM-DA-SP and CLM-PFL-OL, CLM-PFL-DA and CLM-PFL-DA-SP simulations compared to Cosmic-Ray Neutron Sensor measurements for the simulation period of 2018.03.01–2018.11.30.

4.2. Spatial Analysis of OL and DA and SMAP Observations

In the following, we analyze the assimilation effects on spatial patterns of soil moisture (for the upper top 5 cm) for different assimilation scenarios. Figure 7 shows the spatial patterns of modeled soil moisture and their differences with SMAP observations for the simulation period. The CLM-OL simulation consistently produces higher soil moisture than SMAP observations over most of the study area, indicating a systematic positive bias in the CLM model. This overestimation is also present in the CLM-DA and CLM-DA-SP simulations but the deviations are reduced. This suggests that data assimilation is effective in reducing biases and introducing a degree of spatial heterogeneity into the model's output. However, localized assimilation schemes seem to lead to the formation of artificial soil moisture patterns that are related to SMAP footprints.

In contrast, all CLM-ParFlow configurations exhibit a more pronounced spatial heterogeneity in soil moisture compared to CLM and its data assimilation variants. This enhanced heterogeneity reflects the ability of CLM-ParFlow to simulate lateral flow processes that contributes to a more realistic representation of soil moisture distribution, particularly in areas with complex topography. The assimilation of SMAP data in the CLM-PFL-DA and CLM-PFL-DA-SP experiments further modifies the soil moisture patterns, resulting in a more localized variability of soil moisture that aligns better with SMAP observations. Note that the reductions in discrepancies are spatially heterogeneous, for instance, southern areas with complex topography, where lateral flow dominates, tend to benefit more.

10.1029/2024WR038647

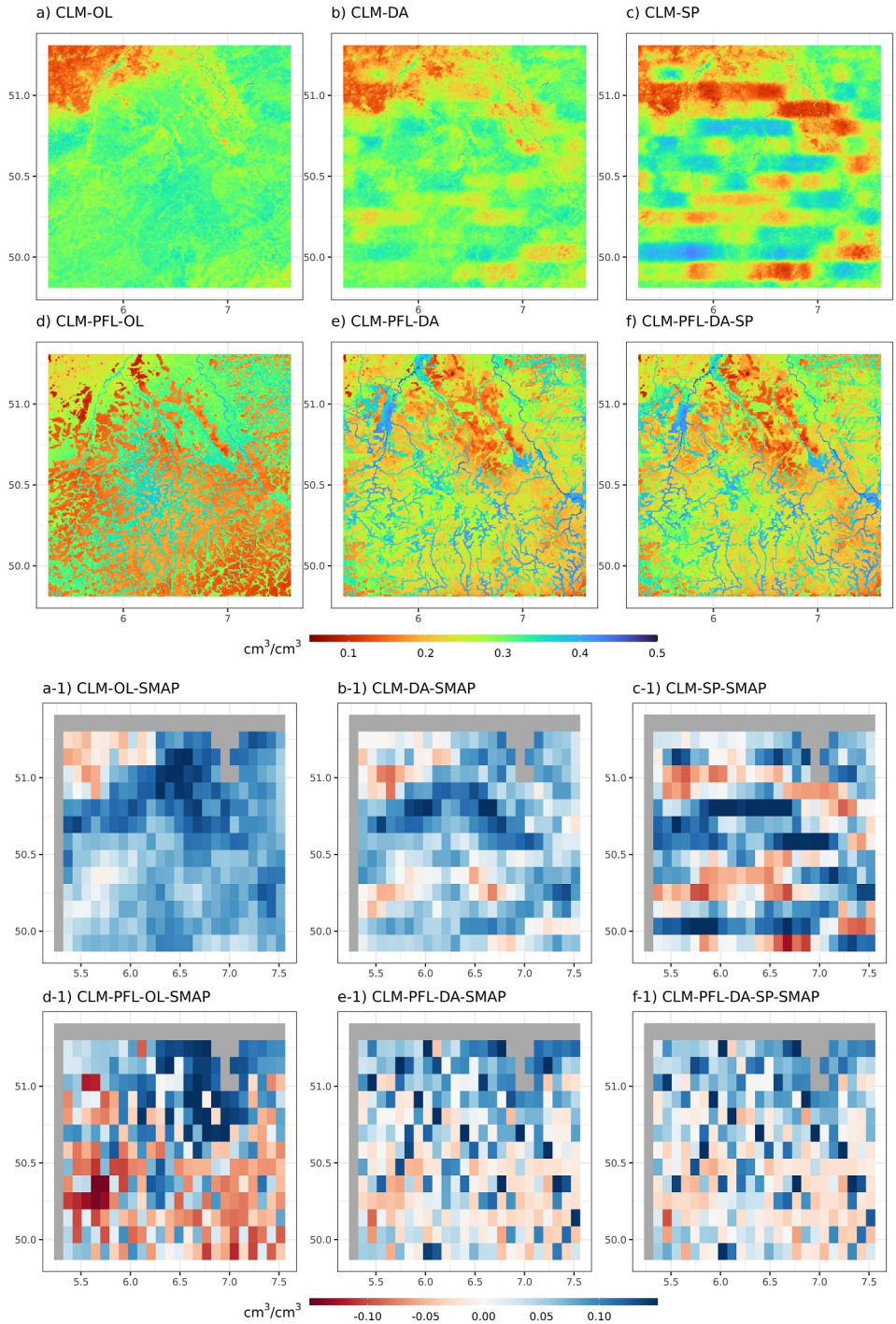

Figure 7. Temporally averaged soil moisture for the period of 2018.03.01–2018.11.30: (a) CLM-OL, (b) CLM-DA, (c) CLM-DA-SP, (d) CLM-PFL-OL, (e) CLM-PFL-DA, and (f) CLM-PFL-DA-SP at model resolution, along with their respective differences compared to Soil Moisture Active Passive (SMAP) observations at SMAP grid resolution a-1) to f-1), where gray areas indicate missing values.

Interestingly, the performance of CLM-PFL-DA and CLM-PFL-DA-SP is very similar, illustrating that parameter estimation does not clearly improve simulation results. This could be attributed to the inherent strengths of the CLM-ParFlow model, which already captures key hydrological processes such as lateral flow in soil moisture redistribution. Additionally, the lack of parameter updates for deep subsurface layers in the assimilation process may limit the potential for further improvements in soil moisture.

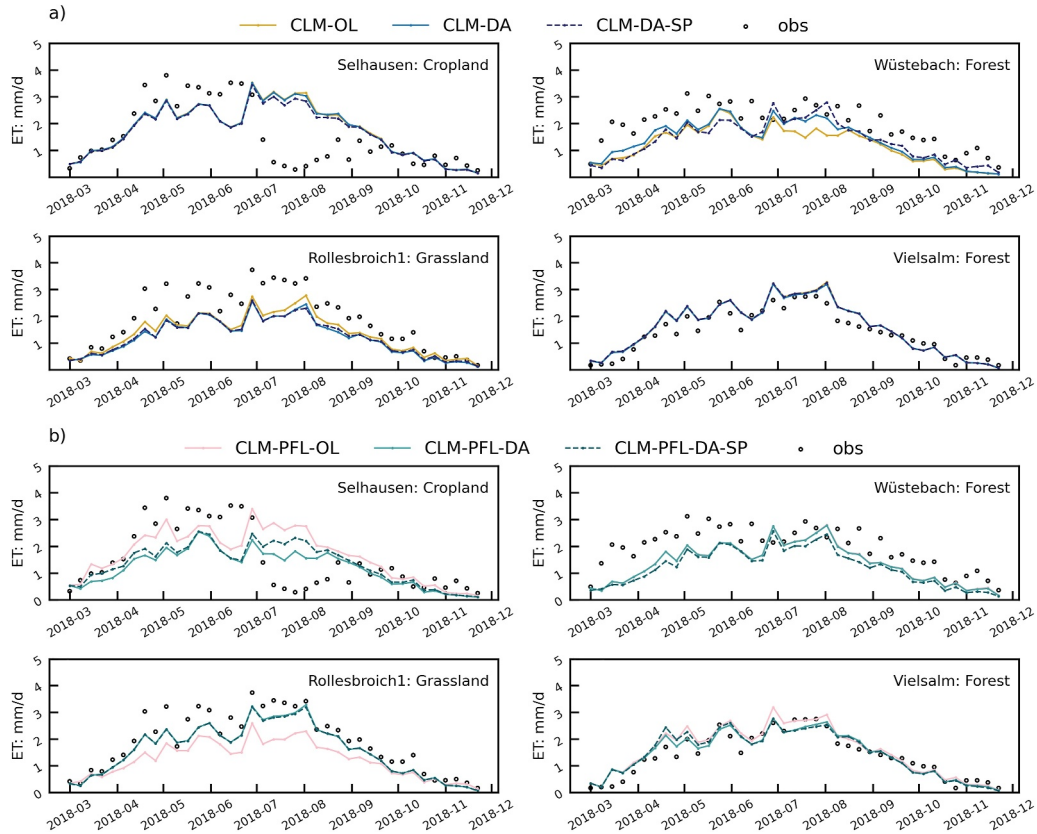

Figure 8. Time series of weekly evapotranspiration simulated by (a) CLM-OL, CLM-DA, CLM-DA-SP, (b) CLM-PFL-OL, CLM-PFL-DA and CLM-PFL-DA-SP compared to in situ measurements at the four eddy-covariance (EC) sites: Selhausen, Wüstebach, Rollesbroich1 and Vielsalm. Black dots represent flux tower observations.

4.3. Evaluation of In Situ Evapotranspiration (ET) Measurements

The influence of soil moisture DA on ET modeling is also investigated. Figure 8 shows the temporal dynamics of daily ET at four EC sites. The simulated ET agrees well with the observations at most EC sites. A seasonal pattern is visible, with higher values corresponding to the growing season with higher incoming radiation and increased vegetation activity. The observed ET shows significant temporal variability, with occasional spikes, which could be due to natural variability in weather patterns, vegetation responses, or measurement errors. The quantitative evaluation metrics of R and ubRMSE are shown in Table 5, where no significant impact of data assimilation is found. For the CLM model, the average r are 0.73, 0.73 and 0.74, and the average ubRMSE are 0.71, 0.71 and 0.70 mm/d for the OL, DA and DA-SP respectively. The coupled CLM-PFL model exhibits similar performance, yielding r values of 0.76, 0.74 and 0.72, and average ubRMSE are observed to be 0.70, 0.71 and 0.73 mm/d for the OL, DA and DA-SP, respectively.

At the Selhausen site, the consistent underestimation of ET by both models during the growing season suggests a potential misrepresentation of the crop cycle dynamics. In situ observations reveal a sharp decline in ET rates following senescence and summer harvesting in combination with very dry conditions at that time. This decline is not captured by either of the models, owing to the absence of harvest-related information in the model scheme and at least in case of CLM stand-alone also an overestimation of the soil moisture content. By comparing Figures 6 and 8, we find that ET and soil moisture are strongly correlated, with changes in soil moisture typically being reflected in corresponding changes in ET. The high ET simulated by CLM-PFL-OL at Selhausen is reduced as soil moisture decreases by the assimilation, which reduces latent heat flux and increases sensible heat flux. The finding aligns with previous research (Martens et al., 2016; Peters-Lidard et al., 2011), which established a strong correlation between the improved or degraded representation of ET fields and the corresponding changes in simulated soil moisture induced by assimilating remote sensing soil moisture products. The only limited

Table 5
Comparison Metrics of Pearson r and Unbiased Root Mean Square Error (mm/d) for the Simulated Evapotranspiration From CLM-OL, CLM-DA, CLM-DA-SP, CLM-PFL-OL, CLM-PFL-DA and CLM-PFL-SP at Four EC Sites for the Period of 2018.03.01–2018.11.30

Stations	Model runs	r	ubRMSE	Model runs	r	ubRMSE
Selhausen	CLM-OL	0.47	1.22	CLM-PFL-OL	0.47	0.94
	CLM-DA	0.47	1.21	CLM-PFL-DA	0.47	1.11
	CLM-DA-SP	0.49	1.17	CLM-PFL-DA-SP	0.49	1.12
Wüstebach	CLM-OL	0.63	0.75	CLM-PFL-OL	0.62	0.75
	CLM-DA	0.63	0.75	CLM-PFL-DA	0.62	0.75
	CLM-DA-SP	0.63	0.75	CLM-PFL-DA-SP	0.62	0.75
Rollesbroich1	CLM-OL	0.92	0.47	CLM-PFL-OL	0.87	0.69
	CLM-DA	0.93	0.48	CLM-PFL-DA	0.91	0.59
	CLM-DA-SP	0.92	0.48	CLM-PFL-DA-SP	0.89	0.64
Vielsalm	CLM-OL	0.90	0.40	CLM-PFL-OL	0.89	0.42
	CLM-DA	0.90	0.40	CLM-PFL-DA	0.90	0.41
	CLM-DA-SP	0.90	0.40	CLM-PFL-DA-SP	0.89	0.42

improvements in ET characterization related to soil moisture data assimilation could be partly due to the limited value of absolute soil moisture data to estimate energy fluxes with LSMs. Other factors, such as incoming shortwave radiation, vegetation schemes, roughness length parameterization, also have a significant impact on the modeled latent and sensible heat fluxes.

4.4. Evaluation of Groundwater Level Simulated by CLM-ParFlow

During the assimilation process, the pressure head is updated based on the Mualem-van Genuchten model (Van Genuchten, 1980), which has an impact on the simulated groundwater levels. The simulated groundwater levels are spatially interpolated from model grid points to the closest location of the monitoring well. Figure 9 illustrates the validation results of mean monthly groundwater levels (in terms of Pearson correlation and RMSE evaluated across 527 sites) for the three simulations with the CLM-ParFlow model. The median Pearson r value for the OL (0.73) is notably higher compared to the value for the DA (0.29) and DA-SP (0.32) experiments, suggesting that the OL experiment without data assimilation already captures the monthly groundwater variation well at many sites. Contrary to the correlation results, the OL, DA and DA-SP have similar median RMSE values of 6.25 m, 6.54 and 6.54 m respectively, suggesting that soil moisture assimilation is not able to improve groundwater depth characterization. One potential explanation is that groundwater wells may be subject to localized influences, which may be related to land use and human activities. The remotely sensed soil moisture data, however, have a

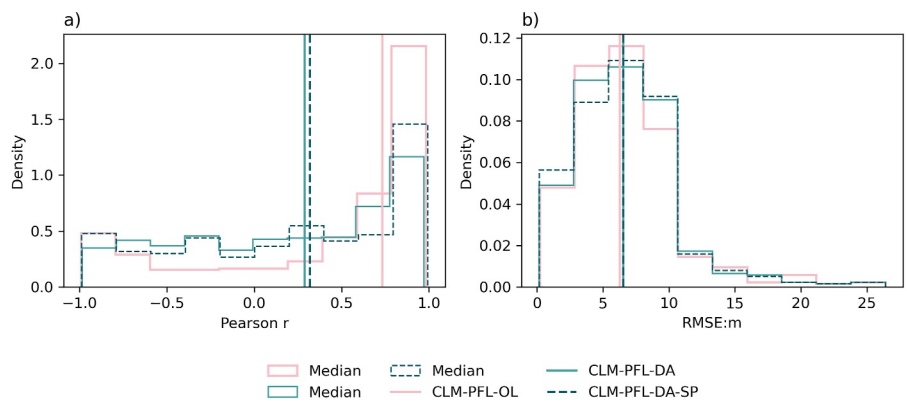

Figure 9. Comparison of model performance metrics across three CLM-PFL scenarios for monthly groundwater level simulations at 527 sites: (a) Pearson r (b) root mean square error).

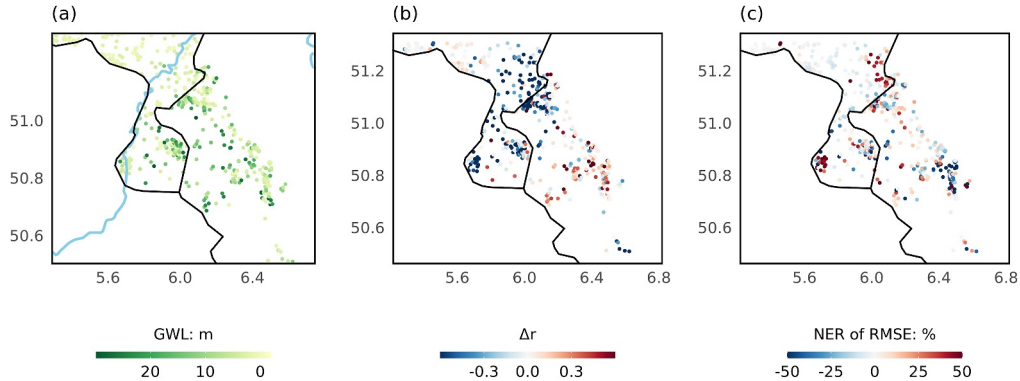

Figure 10. The spatial distribution of (a) observed annual mean groundwater levels, and (b, c) the performance of CLM-PFL-SP simulations compared to CLM-PFL-OL. Performance is evaluated in terms of changes in Pearson r (Δr) and reduction in root mean square error (NER: %).

relatively coarse resolution and are therefore unable to capture this information. The DA-SP experiment appears to have a slightly higher median ubRMSE compared to DA, however, the DA-SP experiment shows a tighter distribution, which suggests that the results are more consistent across different sites.

To further investigate the impact of data assimilation, we present the spatial distribution of Δr and RMSE reduction (NER) for the CLM-PFL-SP compared to CLM-PFL-OL experiments in Figure 10. As there are only minor differences in the performances of CLM-PFL-DA and CLM-PFL-SP, we do not show CLM-PFL-DA here. The spatial analysis of Δr and NER of RMSE shows that only a small portion of sites benefit from data assimilation, indicated by both increased Δr and decreased NER. At most sites, however, the two metrics display an inverse relationship. Regions with decreased Pearson r often coincide with areas where RMSE is notably reduced. One possible explanation is that the groundwater level characterization improves gradually over time, during the simulation period. However, for the overall time series this results in a worse representation of seasonal dynamics (due to the gradual adjustments over time by DA) with an associated worse correlation between simulated and measured values, compared to the OL run.

5. Discussion

The performance metrics show the relatively better performance of data assimilation runs compared to the open loop runs for both CLM and CLM-ParFlow. The SMAP retrievals are characterized by a spatial resolution of 9 km yet exhibit discontinuities in both spatial and temporal coverage. In contrast, both CLM and CLM-ParFlow are run at a high-resolution scale of 500 m, generating continuous predictions. This study supports that SMAP products have significant skill to improve the accuracy and consistency of soil moisture estimations. However, the improvement in soil moisture characterization for CLM-ParFlow is less significant than the improvement for CLM stand-alone in the time series plot (Figure 4). This may be due to the fact that the coupled CLM-ParFlow already simulates soil moisture very well, leaving less room for further improvement. It is important to note that the footprints of SMAP are much larger than the model resolution. In this study, the SMAP soil moisture data are assigned to the nearest model grid cell, and the other surrounding grid cells within a local radius are updated via the covariance. Another possibility is to implement multi-scale assimilation for remote sensing soil moisture products like SMAP. This would allow for the updating of multiple model grid cells covered by a satellite footprint (Montzka et al., 2012). In multi-scale assimilation, the average simulated soil moisture within a satellite footprint is compared with the satellite soil moisture observations, which may result in improved assimilation results for the CLM and CLM-ParFlow models. The spatial variability in soil moisture simulated by CLM is limited due to the CLM model structure, which does not account for lateral water flow processes between adjacent grid cells. The absence of lateral flow processes restricts CLM's ability to capture the influence of topographic features and subsurface heterogeneities on the soil moisture distribution, resulting in spatially uniform soil moisture patterns that deviate from reality.

The results from ET validation generally agree with previous assimilation studies (Gebler et al., 2017; Martens et al., 2016; Peters-Lidard et al., 2011) and also for the same model (Hung et al., 2022; F. Li et al., 2024), that is,

the assimilation of soil moisture only marginally improves the estimation of ET. Larger improvements are found under drier conditions (during the summer period). Note that the southern modeling area is predominantly characterized as energy limited rather than water limited due to the relatively low temperatures and global radiation and high annual precipitation (Section 2.1). ET in such an environment may approach the potential ET, and is mostly controlled by energy availability (e.g., temperature and radiation) rather than soil moisture. The findings align with (Baatz et al., 2017) and (F. Li et al., 2024), where they also found that soil moisture assimilation had minimal effect on ET in the southern part of the area. Studies from Nearing et al. (2016, 2018) concluded that uncertainties in soil moisture characterization are mainly influenced by soil texture, whereas ET predictions are predominantly affected by uncertainties in forcing data. While our findings in the southern part could support this, however, we also find that soil moisture exerts a more important control on ET in the northern part.

In the CLM model, ET is simulated as a function of soil moisture and vegetation parameters, which makes the model more suitable for water-limited conditions. However, to effectively simulate both water- and energy-limited conditions, a scheme should be introduced to consider maximum ET based on available solar radiation. Such a scheme would allow for a better representation of energy-limited environments where ET is predominantly driven by energy availability rather than soil moisture. Moreover, the spatial variability as shown here underscores the critical need for a deeper understanding and improved quantification of the transition between energy-limited and water-limited conditions in LSMs. Such transitions are influenced by the complex interplay of drivers, including meteorological factors and vegetation status (LAI).

In addition, the ET calculation is also largely influenced by uncertainties in atmospheric forcings and vegetation parameters which control root water uptake and stomata closure. To improve ET estimation, it may be beneficial to assimilate other data types such as ET or LAI. Studies have shown that multivariate assimilation of remotely sensed soil moisture and ET (Gavahi et al., 2020) or LAI observations (Albergel et al., 2017; Fairbairn et al., 2017; Rahman et al., 2022) at finer resolutions contributes significantly to improved ET characterization.

Few studies investigate the influence of assimilating soil moisture on groundwater level predictions in a coupled modeling framework at the larger regional scale. A comparison of the modeled groundwater levels with observations from 527 wells revealed that the assimilation of SMAP soil moisture did not result in improvements in the RMSE. An important aspect is the spatial mismatch between the model resolution and SMAP observations, therefore, it may not be appropriate to evaluate the accuracy of the groundwater level simulations based on the well measurements. On the other hand, the groundwater level is controlled by recharge, the aquifer transmissivity, the aquifer geometry, and, to some extent, the topography itself (Haitjema & Mitchell-Bruker, 2005). In this mountainous modelling domain, regional flow is generally stronger than perpendicular flow and is mainly influenced by the ratio of recharge to hydraulic conductivity (Gleeson & Manning, 2008). SMAP measures surface soil moisture, which shows a weak correlation with deeper groundwater aquifers. Therefore, its effectiveness in updating parameters in the deep aquifers is very limited. Additionally, the relatively coarse spatial resolution of SMAP data limits its ability to capture variations caused by lateral flow in the CLM-ParFlow model. This finding is also consistent with Hung et al. (2022), while our real-world case presents more complexity. In the future, better results may be obtained by using a model resolution of 100 m instead of 500 m, which allows for better representation of small valleys. The CLM-ParFlow model is constrained to a vertical depth of 30 m and this simplification does not fully account for the complexity of real-world aquifer systems. Consequently, measurements in deeper aquifers are excluded from the analysis. In future work, extending the vertical depth of the model could enhance the realism of the simulations. Nevertheless, this objective would require a more detailed representation of three-dimensional geological structure to accurately represent the complex layering and interactions within the subsurface.

In both model configurations, we find that joint updating the parameters and states does not provide better results than only updating the states, suggesting that there may be difficulties to update parameters in the high-resolution real-world cases with the remote sensing soil moisture information. The parameter spread (uncertainty) is still large after the assimilation (see Figure 11). Prescribing an inaccurate soil structure could result in deteriorated soil moisture estimates, particularly in sites like Wildenrath, which is characterized by dense forest cover. In such circumstances, the accuracy of SMAP retrieval is subject to large uncertainty. Studies (Zhao et al., 2023) have demonstrated that the retrieval of soil physical properties through the assimilation of remote sensing information is unlikely to enhance the accuracy of modelled soil moisture. Assimilating high quality soil moisture measurements,

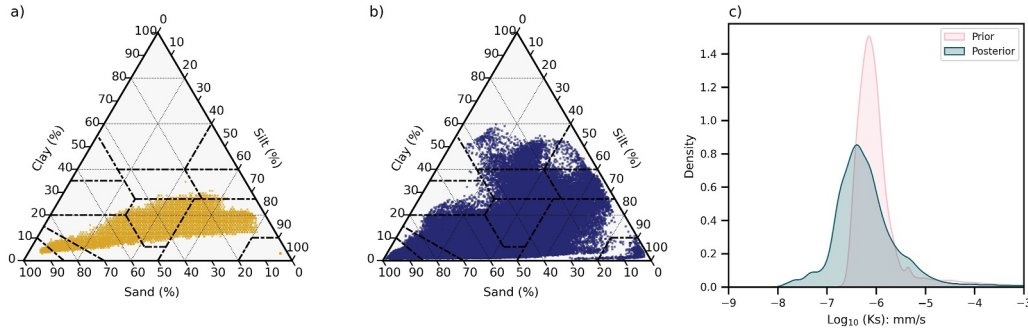

Figure 11. Ternary diagram of (a) prior (CLM-OL) (b) posterior (CLM-DA-SP) soil texture at 5 cm depth in CLM model, and (c) probability density functions of prior (CLM-PFL-OL) and posterior (CLM-PFL-DA-SP) hydraulic conductivity k_r at the same depth in CLM-ParFlow model.

for example, CRNS observations, probably can provide more accurate parameters for the hydrological models (Baatz et al., 2017; F. Li et al., 2024). In this study, as the soil moisture is updated on a daily basis, the updated values may be in close alignment with the SMAP observations. Consequently, only minor changes in the soil properties are observed. Hung et al. (2022) assimilated soil moisture in the CLM-ParFlow model with an ensemble size of 64 for a virtual case, and the results show that parameter estimation only gives an additional slight improvement compared to updating soil moisture alone. Brandhorst and Neuweiler (2022) also investigated the impact of parameter updates with soil moisture assimilation and found that a small spread in the ensembles impedes parameter updates. Hendricks Franssen and Kinzelbach (2008) suggested that 200–500 realizations may be sufficient for successful joint state-parameter estimation with hydrological models. However, a larger ensemble size in this work was not feasible because of the required computational resources when running the coupled land surface-subsurface model at high resolution. For instance, running the CLM-ParFlow model with 32 ensemble members for one year simulation required 250,000 CPU core hours. In the future, a hybrid machine learning (ML) data assimilation approach with an approximation of the model by a ML-based emulator could allow the simulation of larger ensemble sizes which could improve the performance of the data assimilation and parameter estimation. However, we feel that the remotely sensed information might also not be accurate enough to estimate model parameters, especially because the observation is at a coarse scale and limited to the upper few cm of the soil.

One challenge of this study was trying to maintaining the consistent configurations between the CLM and CLM-ParFlow model despite their different representations of the subsurface. To address this, we perturbed the percentages of sand and clay content in a homogeneous manner in the CLM model and employed the Rosetta pedotransfer function to convert these parameters into hydraulic conductivity for the CLM-ParFlow model. The perturbation is spatially uniform and could be improved to consider better the spatial variability of soil characteristics. Additionally, previous studies (Ryu et al., 2009) suggest that input parameters and forcing data can have complicated feedback in the model process, leading to unintended effects of the ensemble perturbation. Investigating more advanced ways to create ensembles for different variables is necessary, but beyond the scope of this study. Additionally, it has been suggested that other parameters (α and n in the van Genuchten model) can be estimated (Chaudhuri et al., 2018; Yetbarek et al., 2020), which was not considered in our study. However, the estimation of α and n would bring more instabilities considering our limited number of ensembles members and the complexity of real-world cases.

It should be noted that the quality check for SMAP retrievals was primarily based on the retrieval quality flag, which did not fully consider the impact of dense vegetation. The SMAP manuel (P. O'Neill et al., 2020) suggests that data with a Vegetation Water Content (VWC) less than 5 kg/m^2 is optimal for retrieval. However, as the research area is largely covered by dense vegetation, observations with a VWC between 5 and 10 kg/m^2 were also used in the assimilation process. As the observations are spatially uniform, this introduces additional uncertainty into the model and affects the predictions, as evidenced by the example of the Wüstebach site. Accurate estimation of observation errors can improve the benefits of assimilating remote sensing products (Degelia & Wang, 2023; Terasaki & Miyoshi, 2024). A possible future work is to consider the spatial patterns of the microwave soil moisture retrievals in order to quantify the observational errors, taking into account sensitivities to vegetation and other atmospheric conditions.

The EnKF is an example of a sequential algorithm, which makes it well-suited to real-time forecasting applications, including hydrological studies, weather prediction, and other modeling tasks. However, the EnKF relies on several underlying assumptions (Evensen, 2003) that may not always hold in practical applications, particularly in complex, high-dimensional land surface systems. A critical aspect of improving EnKF performance—and DA in general—is achieving an optimal balance among model structure, model parameters, observation data and assimilation technique. Research indicates that misrepresentation of model errors (Jafarpour & Tarrahi, 2011; Pathiraja et al., 2018; Reichle et al., 2002) can significantly impact the effectiveness of DA. A study assessing the assimilation of satellite-derived SM retrievals over irrigated areas in the U.S. demonstrated that the success of DA largely depended on the model bias (S. Kumar et al., 2015). Additionally, LSMs often misrepresent the coupling between SM and ET or runoff, leading to reduced DA performance in constraining water fluxes using SM observations (Crow et al., 2024). Future research should focus on enhancing the understanding and refinement of LSMs parameterization to further improve DA efficiency.

6. Conclusions

In this study, the remote sensing SMAP soil moisture product is assimilated into the Community Land Model (CLM 3.5) and the coupled land surface-subsurface model CLM-ParFlow (CLM-PFL) over a region of size 22.500 km^2 in western Germany for the year of 2018. A total of 32 ensemble members is generated by perturbing the atmospheric forcings (for both the CLM and CLM-ParFlow model), soil texture properties (for CLM) and hydraulic conductivity and porosity (for CLM-ParFlow). The DA experiments are carried out with the LEnKF and SMAP data are assimilated daily. The characterization of soil moisture and other hydrological variables are then assessed with in situ measurements. The key messages from this study and the recommendations for future research are as follows:

1. The assimilation of SMAP soil moisture observations into the CLM and CLM-ParFlow generally improves the soil moisture characterization with an increase of the median Pearson correlation from 0.72 to 0.79 (CLM) and 0.79 to 0.83 (CLM-PFL) and a reduction of the median ubRMSE from 0.063 to 0.060 cm^3/cm^3 (CLM) and 0.050 to 0.046 cm^3/cm^3 (CLM-PFL). The coupled model shows greater soil moisture spatial variability that is closer to reality, showing that the consideration of lateral flow dynamics is crucial for a realistic simulation of soil moisture. These advantages cannot be fully offset by assimilating soil moisture in CLM.
2. However, the assimilation of soil moisture data does not improve the ET characterization compared to the open loop runs for both CLM and CLM-ParFlow, which may be attributed to the energy-limited conditions within the modeling domain. When compared to monthly groundwater level measurements, the assimilation does not reduce the RMSE and the correlation between simulated and measured groundwater levels even decreases. This outcome suggests that assimilating surface soil moisture alone is insufficient to improve groundwater level simulations, likely due to the inherent complexity of groundwater systems and the multitude of controlling factors beyond recharge. It is assumed that more accurate soil moisture data will provide more information to the models. The impact of assimilation passive and active microwave soil moisture data, either individually or in combination, on the predictive skills of the models can be evaluated. Furthermore, we acknowledge the importance of a higher spatial resolution of soil moisture observations, which indicates the need to investigate the assimilation of data from sources such as Sentinel-1 or down-scaled SMAP products. On the other hand, a single measurement type (in this case, soil moisture) may not be sufficient to infer other model states in a complex coupled model. Building on previous studies, which have demonstrated the effectiveness of multivariate data assimilation in LSMs, future research will explore the integration of additional variables—such as LAI or Total Water Storage (TWS)—to further constrain multiple model variables and enhance performance within a coupled land surface-subsurface framework.
3. In this work, we also assimilated soil moisture including parameter estimation and found that joint state parameter estimation does not improve predictions compared to state estimation alone. This might point to the difficulty of using the remotely sensed soil moisture information to improve parameter estimates over a large domain with a complex topography. It would be beneficial to further investigate by utilizing larger ensemble sizes and a more refined computational model once enhanced computational efficiency has been achieved.

Appendix A

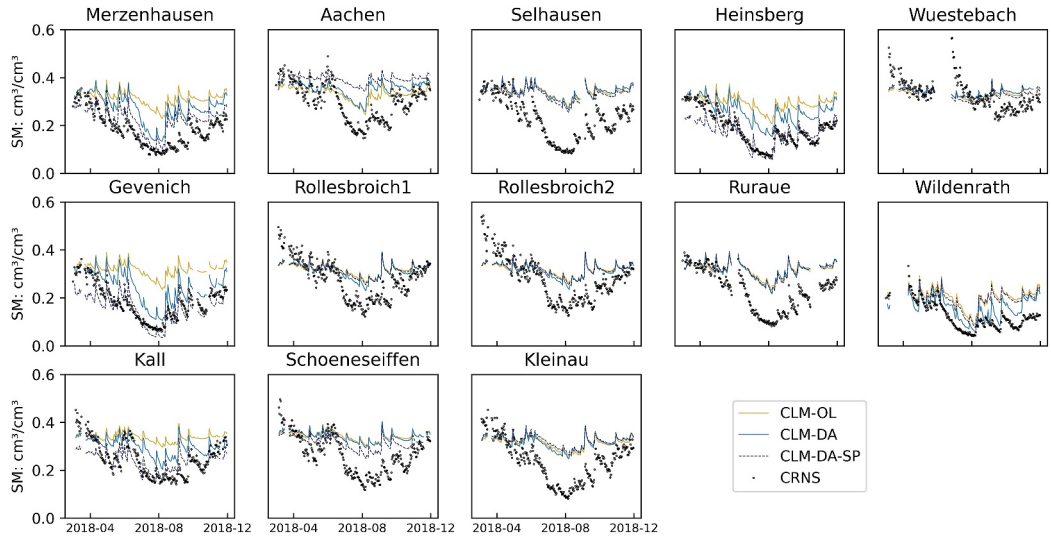

Figure A1. Time series of simulated daily soil moisture (at the depth corresponding to the Cosmic-Ray Neutron Sensor (CRNS)) at 13 CRNS sites for the CLM-OL, CLM-DA and CLM-DA-SP simulation experiments and the period 2018.03.01–2018.11.30. The CRNS observations are shown in black circles.

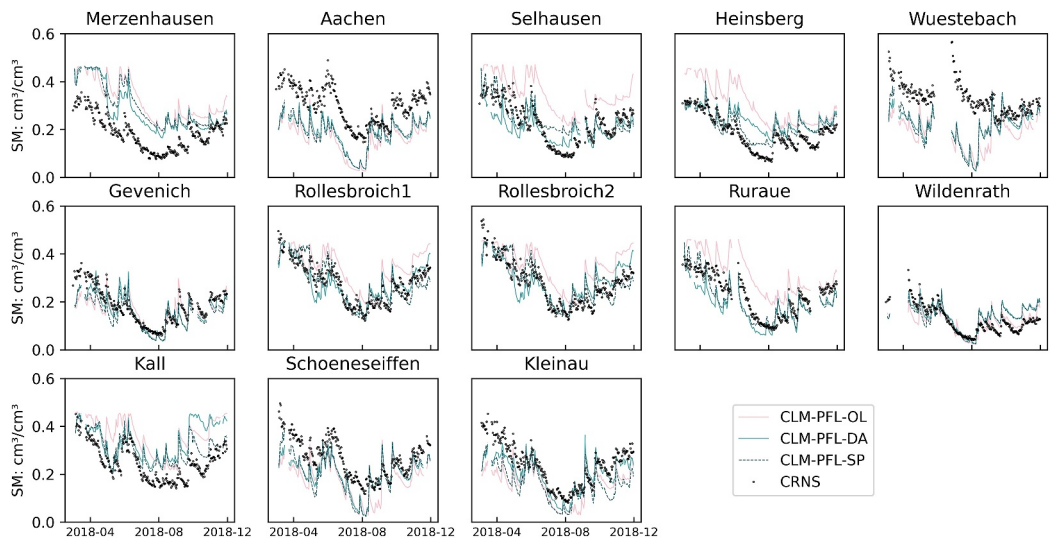

Figure A2. Time series of simulated daily soil moisture (at the depth corresponding to the Cosmic-Ray Neutron Sensor (CRNS)) at 13 CRNS sites for the CLM-PFL-OL, CLM-PFL-DA and CLM-PFL-DA-SP simulations and for the period 2018.03.01–2018.11.30. The CRNS observations are shown in black circles.

Data Availability Statement

The atmospheric reanalysis data set COSMO-REA6 (Bollmeyer et al., 2015) was downloaded from the opendata-FTP server at DWD https://opendata.dwd.de/climate_environment/REA/COSMO_REA6/ (Bollmeyer et al., 2024). The soil texture information and permeability information were described in the paper by Shrestha et al. (2014) and Boas et al. (2023). The SMAP soil moisture was retrieved from https://www.earthdata.nasa.gov/data/instruments/smap-l-band-radiometer (NASA National Snow Ice Data Center Distributed Active Archive and Center & National Snow Ice Data and Center, 2024). The in situ soil moisture (H. R. Bogena et al., 2022) and eddy covariance data set was obtained from https://ddp.tereno.net/ddp/ (last access: 20 December 2024) (H. Bogena & Ney, 2021). The groundwater measurements are freely available at https://www.geoportal.nrw/?activetab=portal (last access: 20 December 2024) and https://www.grondwatertools.nl (last access: 20 December 2024). *Software Availability Statement*: The TSMP framework is detailed in Shrestha et al. (2014) and Gasper et al. (2014). Its repository is open-source and available on GitHub at https://github.com/HPSCTerrSys/TSMP (Hartick et al., 2023). PDAF version 1.13.2 is available for download following registration at http://pdaf.awi.de/trac/wiki (Nerger, 2023). The pedotransfer function (Rosseta) Python package is included in (Y. Zhang & Schaap, 2017), under GPLv2+ licence and accessible at https://github.com/usda-ars-ussl/rosetta-soil (Marcel G. Schaap, 2016). Additional Python package such as pftools at https://github.com/parflow/parflow (Smith et al., 2019) was also used for data processing.

Acknowledgments

We are grateful to the Terrestrial Environmental Observatories (TERENO) community for providing the measurement data. We also extend our thanks to the JUWELS supercomputer at Forschungszentrum Jülich for providing the storage and computational resources. H.Z acknowledges the support of the China Scholarship Council (201806010358), the Dragon 5 cooperation between the European Space Agency and the Ministry of Science and Technology of the P.R. China (Grant 59316) and the DETECT project funded by the Deutsche Forschungsgemeinschaft (DFG, German Research Foundation)-SFB 1502/1-2022–Project number: 450058266. C. M. and H. J.H.F. acknowledge funding by the German Ministry of Economic Affairs and Climate (BMWK) through the German Aerospace Center for the AssimEO project (50EE1914A). F.L acknowledges funding by the China Scholarship Council (201904910448). Open Access funding enabled and organized by Projekt DEAL.

References

Ahmad, J. A., Forman, B. A., & Kumar, S. V. (2022). Soil moisture estimation in south Asia via assimilation of SMAP retrievals. *Hydrology and Earth System Sciences*, *26*(8), 2221–2243. https://doi.org/10.5194/hess-26-2221-2022

Ajami, H., McCabe, M. F., Evans, J. P., & Stisen, S. (2014). Assessing the impact of model spin-up on surface water-groundwater interactions using an integrated hydrologic model. *Water Resources Research*, *50*(3), 2636–2656. https://doi.org/10.1002/2013wr014258

Albergel, C., Dutra, E., Munier, S., Calvet, J.-C., Munoz-Sabater, J., de Rosnay, P., & Balsamo, G. (2018). ERA-5 and ERA-interim driven ISBA land surface model simulations: Which one performs better? *Hydrology and Earth System Sciences*, *22*(6), 3515–3532. https://doi.org/10.5194/hess-22-3515-2018

Albergel, C., Munier, S., Leroux, D. J., Dewaele, H., Fairbairn, D., Barbu, A. L., et al. (2017). Sequential assimilation of satellite-derived vegetation and soil moisture products using SURFEX_v8. 0: LDAS-Monde assessment over the Euro-Mediterranean area. *Geoscientific Model Development*, *10*(10), 3889–3912. https://doi.org/10.5194/gmd-10-3889-2017

Baatz, R., Hendricks Franssen, H.-J., Han, X., Hoar, T., Bogena, H. R., & Vereecken, H. (2017). Evaluation of a cosmic-ray neutron sensor network for improved land surface model prediction. *Hydrology and Earth System Sciences*, *21*(5), 2509–2530. https://doi.org/10.5194/hess-21-2509-2017

Babaeian, E., Sadeghi, M., Jones, S. B., Montzka, C., Vereecken, H., & Tuller, M. (2019). Ground, proximal, and satellite remote sensing of soil moisture. *Reviews of Geophysics*, *57*(2), 530–616. https://doi.org/10.1029/2018rg000618

Baldauf, M., Seifert, A., Förstner, J., Majewski, D., Raschendorfer, M., & Reinhardt, T. (2011). Operational convective-scale numerical weather prediction with the COSMO model: Description and sensitivities. *Monthly Weather Review*, *139*(12), 3887–3905. https://doi.org/10.1175/mwr-d-10-05013.1

Bastidas, L. A., Gupta, H. V., Hsu, K.-L., & Sorooshian, S. (2003). Parameter, structure, and model performance evaluation for land-surface schemes. *Calibration of watershed models*, *6*, 229–237. https://doi.org/10.1029/ws006p0229

Beven, K. J., & Kirkby, M. J. (1979). A physically based, variable contributing area model of basin hydrology/un modèle à base physique de zone d'Appel variable de l'hydrologie du bassin versant. *Hydrological Sciences Journal*, *24*(1), 43–69. https://doi.org/10.1080/02626667909491834

Blyverket, J., Hamer, P. D., Bertino, L., Albergel, C., Fairbairn, D., & Lahoz, W. A. (2019). An evaluation of the EnKF vs. EnOI and the assimilation of SMAP, SMOS and ESA CCI soil moisture data over the contiguous US. *Remote Sensing*, *11*(5), 478. https://doi.org/10.3390/rs11050478

Boas, T., Bogena, H. R., Ryu, D., Vereecken, H., Western, A., & Hendricks Franssen, H.-J. (2023). Seasonal soil moisture and crop yield prediction with fifth-generation seasonal forecasting system (SEAS5) long-range meteorological forecasts in a land surface modelling approach. *Hydrology and Earth System Sciences*, *27*(16), 3143–3167. https://doi.org/10.5194/hess-27-3143-2023

Bogena, H., Huisman, J., Baatz, R., Hendricks Franssen, H.-J., & Vereecken, H. (2013). Accuracy of the cosmic-ray soil water content probe in humid forest ecosystems: The worst case scenario. *Water Resources Research*, *49*(9), 5778–5791. https://doi.org/10.1002/wrcr.20463

Bogena, H., & Ney, P. (2021). Dataset of "COSMOS-Europe: A European network of cosmic-ray neutron soil moisture sensors" [Dataset]. *Forschungszentrum Jülich*. https://doi.org/10.34731/x9s3-kr48

Bogena, H. R., Schrön, M., Jakobi, J., Ney, P., Zacharias, S., Andreasen, M., et al. (2022). Cosmos-Europe: A European network of cosmic-ray neutron soil moisture sensors. *Earth System Science Data*, *14*(3), 1125–1151. https://doi.org/10.5194/essd-14-1125-2022

Bollmeyer, C., Keller, J., Ohlwein, C., Hense, A., Borsche, M., Niermann, D., et al. (2024). Regional reanalysis COSMO-REA6 - Standardised parameters [Dataset]. *World Data Center for Climate (WDCC) at DKRZ*. https://doi.org/10.26050/WDCC/CR6_EU6

Bollmeyer, C., Keller, J., Ohlwein, C., Wahl, S., Crewell, S., Friederichs, P., et al. (2015). Towards a high-resolution regional reanalysis for the European CORDEX domain. *Quarterly Journal of the Royal Meteorological Society*, *141*(686), 1–15. https://doi.org/10.1002/qj.2486

Brandhorst, N., & Neuweiler, I. (2022). Impact of parameter updates on soil moisture assimilation in a 3D heterogeneous hillslope model. *Hydrology and Earth System Sciences Discussions*, *2022*, 1–34.

Chan, S., Bindlish, R., O'Neill, P., Jackson, T., Chaubell, J., Piepmeier, J., et al. (2017). Development and validation of the SMAP enhanced passive soil moisture product. In *2017 ieee international geoscience and remote sensing symposium (igarss)* (pp. 2539–2542).

Chaudhuri, A., Franssen, H.-J. H., & Sekhar, M. (2018). Iterative filter based estimation of fully 3D heterogeneous fields of permeability and Mualem-van Genuchten parameters. *Advances in Water Resources*, *122*, 340–354. https://doi.org/10.1016/j.advwatres.2018.10.023

Clapp, R. B., & Hornberger, G. M. (1978). Empirical equations for some soil hydraulic properties. *Water Resources Research*, *14*(4), 601–604. https://doi.org/10.1029/wr014i004p00601

Clewley, D., Whitcomb, J. B., Akbar, R., Silva, A. R., Berg, A., Adams, J. R., et al. (2017). A method for upscaling in situ soil moisture measurements to satellite footprint scale using random forests. *IEEE Journal of Selected Topics in Applied Earth Observations and Remote Sensing*, *10*(6), 2663–2673. https://doi.org/10.1109/jstars.2017.2690220

Colliander, A., Cosh, M. H., Misra, S., Jackson, T. J., Crow, W. T., Chan, S., et al. (2017). Validation and scaling of soil moisture in a semi-arid environment: SMAP validation experiment 2015 (smapvex15). *Remote Sensing of Environment*, *196*, 101–112. https://doi.org/10.1016/j.rse.2017.04.022

Colliander, A., Reichle, R. H., Crow, W. T., Cosh, M. H., Chen, F., Chan, S., et al. (2021). Validation of soil moisture data products from the NASA SMAP mission. *Ieee Journal of Selected Topics in Applied Earth Observations and Remote Sensing*, *15*, 364–392. https://doi.org/10.1109/jstars.2021.3124743

Cosby, B., Hornberger, G., Clapp, R., & Ginn, T. (1984). A statistical exploration of the relationships of soil moisture characteristics to the physical properties of soils. *Water Resources Research*, *20*(6), 682–690. https://doi.org/10.1029/wr020i006p00682

Crow, W. T., Kim, H., & Kumar, S. (2024). Systematic modeling errors undermine the application of land data assimilation systems for hydrological and weather forecasting. *Journal of Hydrometeorology*, *25*(1), 3–26. https://doi.org/10.1175/jhm-d-23-0069.1

Dee, D. P., Uppala, S. M., Simmons, A. J., Berrisford, P., Poli, P., Kobayashi, S., et al. (2011). The era-interim reanalysis: Configuration and performance of the data assimilation system. *Quarterly Journal of the Royal Meteorological Society*, *137*(656), 553–597. https://doi.org/10.1002/qj.828

Degelia, S. K., & Wang, X. (2023). Impacts of methods for estimating the observation error variance for the frequent assimilation of thermodynamic profilers on convective-scale forecasts. *Monthly Weather Review*, *151*(4), 855–875. https://doi.org/10.1175/mwr-d-21-0049.1

De Lannoy, G. J., & Reichle, R. H. (2016). Assimilation of SMOS brightness temperatures or soil moisture retrievals into a land surface model. *Hydrology and Earth System Sciences*, *20*(12), 4895–4911. https://doi.org/10.5194/hess-20-4895-2016

De Santis, D., Biondi, D., Crow, W., Camici, S., Modanesi, S., Brocca, L., & Massari, C. (2021). Assimilation of satellite soil moisture products for river flow prediction: An extensive experiment in over 700 catchments throughout Europe. *Water Resources Research*, *57*(6), e2021WR029643. https://doi.org/10.1029/2021wr029643

Entekhabi, D., Njoku, E. G., O'neill, P. E., Kellogg, K. H., Crow, W. T., Edelstein, W. N., et al. (2010). The soil moisture active passive (SMAP) mission. *Proceedings of the IEEE*, *98*(5), 704–716. https://doi.org/10.1109/jproc.2010.2043918

Evensen, G. (1994). Sequential data assimilation with a nonlinear quasi-geostrophic model using Monte Carlo methods to forecast error statistics. *Journal of Geophysical Research: Oceans*, *99*(C5), 10143–10162. https://doi.org/10.1029/94jc00572

Evensen, G. (2003). The ensemble kalman filter: Theoretical formulation and practical implementation. *Ocean Dynamics*, *53*(4), 343–367. https://doi.org/10.1007/s10236-003-0036-9

Fairbairn, D., Barbu, A. L., Napoly, A., Albergel, C., Mahfouf, J.-F., & Calvet, J.-C. (2017). The effect of satellite-derived surface soil moisture and leaf area index land data assimilation on streamflow simulations over France. *Hydrology and Earth System Sciences*, *21*(4), 2015–2033. https://doi.org/10.5194/hess-21-2015-2017

Franz, T. E., Zreda, M., Ferre, T., Rosolem, R., Zweck, C., Stillman, S., et al. (2012). Measurement depth of the cosmic ray soil moisture probe affected by hydrogen from various sources. *Water Resources Research*, *48*(8). https://doi.org/10.1029/2012wr011871

Gaspari, G., & Cohn, S. E. (1999). Construction of correlation functions in two and three dimensions. *Quarterly Journal of the Royal Meteorological Society*, *125*(554), 723–757. https://doi.org/10.1002/qj.49712555417

Gasper, F., Görgen, K., Shrestha, P., Sulis, M., Rihani, J., Geimer, M., & Kollet, S. (2014). Implementation and scaling of the fully coupled Terrestrial Systems Modeling Platform (TerrSysMP v1. 0) in a massively parallel supercomputing environment–a case study on JUQUEEN (IBM Blue Gene/Q). *Geoscientific Model Development*, *7*(5), 2531–2543. https://doi.org/10.5194/gmd-7-2531-2014

Gavahi, K., Abbaszadeh, P., Moradkhani, H., Zhan, X., & Hain, C. (2020). Multivariate assimilation of remotely sensed soil moisture and evapotranspiration for drought monitoring. *Journal of Hydrometeorology*, *21*(10), 2293–2308. https://doi.org/10.1175/jhm-d-20-0057.1

Gebler, S., Franssen, H.-J. H., Kollet, S., Qu, W., & Vereecken, H. (2017). High resolution modelling of soil moisture patterns with TerrSysMP: A comparison with sensor network data. *Journal of Hydrology*, *547*, 309–331. https://doi.org/10.1016/j.jhydrol.2017.01.048

Gleeson, T., & Manning, A. H. (2008). Regional groundwater flow in mountainous terrain: Three-dimensional simulations of topographic and hydrogeologic controls. *Water Resources Research*, *44*(10). https://doi.org/10.1029/2008wr006848

Gleeson, T., Smith, L., Moosdorf, N., Hartmann, J., Dürr, H. H., Manning, A. H., et al. (2011). Mapping permeability over the surface of the earth. *Geophysical Research Letters*, *38*(2). https://doi.org/10.1029/2010gl045565

Gruber, A., De Lannoy, G., Albergel, C., Al-Yaari, A., Brocca, L., Calvet, J.-C., et al. (2020). Validation practices for satellite soil moisture retrievals: What are (the) errors? *Remote Sensing of Environment*, *244*, 111806. https://doi.org/10.1016/j.rse.2020.111806

Haitjema, H. M., & Mitchell-Bruker, S. (2005). Are water tables a subdued replica of the topography? *Groundwater Series*, *43*(6), 781–786. https://doi.org/10.1111/j.1745-6584.2005.00090.x

Han, X., Franssen, H.-J. H., Montzka, C., & Vereecken, H. (2014). Soil moisture and soil properties estimation in the community land model with synthetic brightness temperature observations. *Water Resources Research*, *50*(7), 6081–6105. https://doi.org/10.1002/2013wr014586

Han, X., Hendricks Franssen, H.-J., Li, X., Zhang, Y., Montzka, C., & Vereecken, H. (2013). Joint assimilation of surface temperature and l-band microwave brightness temperature in land data assimilation. *Vadose Zone Journal*, *12*(3), 1–16. https://doi.org/10.2136/vzj2012.0072

Hartick, C., Poll, S., Keller, J., Wagner, N., Benke, J., Caviedes-Voullième, D., et al. (2023). TSMP [Software]. *Zenodo*. https://doi.org/10.5281/zenodo.8283716

Hartley, A., MacBean, N., Georgievski, G., & Bontemps, S. (2017). Uncertainty in plant functional type distributions and its impact on land surface models. *Remote Sensing of Environment*, *203*, 71–89. https://doi.org/10.1016/j.rse.2017.07.037

Hendricks Franssen, H.-J., & Kinzelbach, W. (2008). Real-time groundwater flow modeling with the ensemble Kalman filter: Joint estimation of states and parameters and the filter inbreeding problem. *Water Resources Research*, *44*(9). https://doi.org/10.1029/2007wr006505

Hengl, T., De Jesus, J. M., MacMillan, R. A., Batjes, N. H., Heuvelink, G. B., Ribeiro, E., et al. (2014). SoilGrids1km—Global soil information based on automated mapping. *PLoS One*, *9*(8), e105992. https://doi.org/10.1371/journal.pone.0105992

Hengl, T., Mendes de Jesus, J., Heuvelink, G. B., Ruiperez Gonzalez, M., Kilibarda, M., Blagotić, A., et al. (2017). SoilGrids250m: Global gridded soil information based on machine learning. *PLoS One*, *12*(2), e0169748. https://doi.org/10.1371/journal.pone.0169748

Holtzman, N. M., Pavelsky, T. M., Cohen, J. S., Wrzesien, M. L., & Herman, J. D. (2020). Tailoring WRF and Noah-MP to improve process representation of Sierra Nevada runoff: Diagnostic evaluation and applications. *Journal of Advances in Modeling Earth Systems*, *12*(3), e2019MS001832. https://doi.org/10.1029/2019ms001832

Houtekamer, P. L., & Mitchell, H. L. (1998). Data assimilation using an ensemble Kalman filter technique. *Monthly Weather Review*, *126*(3), 796–811. https://doi.org/10.1175/1520-0493(1998)126<0796:dauaek>2.0.co;2

Hung, C. P., Schalge, B., Baroni, G., Vereecken, H., & Hendricks Franssen, H.-J. (2022). Assimilation of groundwater level and soil moisture data in an integrated land surface-subsurface model for southwestern Germany. *Water Resources Research*, *58*(6), e2021WR031549. https://doi.org/10.1029/2021wr031549

Hunt, B. R., Kostelich, E. J., & Szunyogh, I. (2007). Efficient data assimilation for spatiotemporal chaos: A local ensemble transform Kalman filter. *Physica D: Nonlinear Phenomena*, *230*(1–2), 112–126. https://doi.org/10.1016/j.physd.2006.11.008

Jafarpour, B., & Tarrahi, M. (2011). Assessing the performance of the ensemble Kalman filter for subsurface flow data integration under variogram uncertainty. *Water Resources Research*, *47*(5). https://doi.org/10.1029/2010wr009090

Jakobi, J., Huisman, J., Vereecken, H., Diekkrüger, B., & Bogena, H. (2018). Cosmic ray neutron sensing for simultaneous soil water content and biomass quantification in drought conditions. *Water Resources Research*, *54*(10), 7383–7402. https://doi.org/10.1029/2018wr022692

Jha, M. K., Chowdhury, A., Chowdary, V., & Peiffer, S. (2007). Groundwater management and development by integrated remote sensing and geographic information systems: Prospects and constraints. *Water Resources Management*, *21*(2), 427–467. https://doi.org/10.1007/s11269-006-9024-4

Kerr, Y. H., Waldteufel, P., Wigneron, J.-P., Delwart, S., Cabot, F., Boutin, J., et al. (2010). The SMOS mission: New tool for monitoring key elements of the global water cycle. *Proceedings of the IEEE*, *98*(5), 666–687. https://doi.org/10.1109/jproc.2010.2043032

Kim, J., & Mohanty, B. P. (2017). A physically based hydrological connectivity algorithm for describing spatial patterns of soil moisture in the unsaturated zone. *Journal of Geophysical Research: Atmospheres*, *122*(4), 2096–2114. https://doi.org/10.1002/2016jd025591

Koch, J., Cornelissen, T., Fang, Z., Bogena, H., Diekkrüger, B., Kollet, S., & Stisen, S. (2016). Inter-comparison of three distributed hydrological models with respect to seasonal variability of soil moisture patterns at a small forested catchment. *Journal of Hydrology*, *533*, 234–249. https://doi.org/10.1016/j.jhydrol.2015.12.002

Köhli, M., Schrön, M., Zreda, M., Schmidt, U., Dietrich, P., & Zacharias, S. (2015). Footprint characteristics revised for field-scale soil moisture monitoring with cosmic-ray neutrons. *Water Resources Research*, *51*(7), 5772–5790. https://doi.org/10.1002/2015wr017169

Kollet, S. J., & Maxwell, R. M. (2006). Integrated surface–groundwater flow modeling: A free-surface overland flow boundary condition in a parallel groundwater flow model. *Advances in Water Resources*, *29*(7), 945–958. https://doi.org/10.1016/j.advwatres.2005.08.006

Kollet, S. J., & Maxwell, R. M. (2008). Capturing the influence of groundwater dynamics on land surface processes using an integrated, distributed watershed model. *Water Resources Research*, *44*(2). https://doi.org/10.1029/2007wr006004

Konings, A. G., Piles, M., Das, N., & Entekhabi, D. (2017). L-band vegetation optical depth and effective scattering albedo estimation from SMAP. *Remote Sensing of Environment*, *198*, 460–470. https://doi.org/10.1016/j.rse.2017.06.037

Koster, R. D., Liu, Q., Mahanama, S. P., & Reichle, R. H. (2018). Improved hydrological simulation using SMAP data: Relative impacts of model calibration and data assimilation. *Journal of Hydrometeorology*, *19*(4), 727–741. https://doi.org/10.1175/jhm-d-17-0228.1

Kumar, S., Peters-Lidard, C., Santanello, J., Reichle, R., Draper, C., Koster, R., et al. (2015). Evaluating the utility of satellite soil moisture retrievals over irrigated areas and the ability of land data assimilation methods to correct for unmodeled processes. *Hydrology and Earth System Sciences*, *19*(11), 4463–4478. https://doi.org/10.5194/hess-19-4463-2015

Kumar, S. V., Reichle, R. H., Koster, R. D., Crow, W. T., & Peters-Lidard, C. D. (2009). Role of subsurface physics in the assimilation of surface soil moisture observations. *Journal of Hydrometeorology*, *10*(6), 1534–1547. https://doi.org/10.1175/2009jhm1134.1

Kurtz, W., He, G., Kollet, S. J., Maxwell, R. M., Vereecken, H., & Hendricks Franssen, H.-J. (2016). TerrSysMP–PDAF (version 1.0): A modular high-performance data assimilation framework for an integrated land surface–subsurface model. *Geoscientific Model Development*, *9*(4), 1341–1360. https://doi.org/10.5194/gmd-9-1341-2016

Laguë, M. M., Bonan, G. B., & Swann, A. L. (2019). Separating the impact of individual land surface properties on the terrestrial surface energy budget in both the coupled and uncoupled land–atmosphere system. *Journal of Climate*, *32*(18), 5725–5744. https://doi.org/10.1175/jcli-d-18-0812.1

Li, F., Bogena, H. R., Bayat, B., Kurtz, W., & Hendricks Franssen, H.-J. (2024). Can a sparse network of cosmic ray neutron sensors improve soil moisture and evapotranspiration estimation at the larger catchment scale? *Water Resources Research*, *60*(1), e2023WR035056. https://doi.org/10.1029/2023wr035056

Li, J., Chen, F., Zhang, G., Barlage, M., Gan, Y., Xin, Y., & Wang, C. (2018). Impacts of land cover and soil texture uncertainty on land model simulations over the central Tibetan plateau. *Journal of Advances in Modeling Earth Systems*, *10*(9), 2121–2146. https://doi.org/10.1029/2018ms001377

Liang, X., Xie, Z., & Huang, M. (2003). A new parameterization for surface and groundwater interactions and its impact on water budgets with the variable infiltration capacity (VIC) land surface model. *Journal of Geophysical Research: Atmospheres*, *108*(D16). https://doi.org/10.1029/2002jd003090

Lievens, H., De Lannoy, G., Al Bitar, A., Drusch, M., Dumedah, G., Franssen, H.-J. H., et al. (2016). Assimilation of SMOS soil moisture and brightness temperature products into a land surface model. *Remote Sensing of Environment*, *180*, 292–304. https://doi.org/10.1016/j.rse.2015.10.033

Lievens, H., Martens, B., Verhoest, N., Hahn, S., Reichle, R., & Miralles, D. G. (2017). Assimilation of global radar backscatter and radiometer brightness temperature observations to improve soil moisture and land evaporation estimates. *Remote Sensing of Environment*, *189*, 194–210. https://doi.org/10.1016/j.rse.2016.11.022

Lievens, H., Reichle, R. H., Liu, Q., De Lannoy, G. J., Dunbar, R. S., Kim, S., et al. (2017). Joint sentinel-1 and SMAP data assimilation to improve soil moisture estimates. *Geophysical Research Letters*, *44*(12), 6145–6153. https://doi.org/10.1002/2017gl073904

Lu, Y., Steele-Dunne, S. C., & De Lannoy, G. J. (2020). Improving soil moisture and surface turbulent heat flux estimates by assimilation of SMAP brightness temperatures or soil moisture retrievals and goes land surface temperature retrievals. *Journal of Hydrometeorology*, *21*(2), 183–203. https://doi.org/10.1175/jhm-d-19-0130.1

Martens, B., Miralles, D., Lievens, H., Fernández-Prieto, D., & Verhoest, N. E. (2016). Improving terrestrial evaporation estimates over continental Australia through assimilation of SMOS soil moisture. *International Journal of Applied Earth Observation and Geoinformation*, *48*, 146–162. https://doi.org/10.1016/j.jag.2015.09.012

Maxwell, R. M. (2013). A terrain-following grid transform and preconditioner for parallel, large-scale, integrated hydrologic modeling. *Advances in Water Resources*, *53*, 109–117. https://doi.org/10.1016/j.advwatres.2012.10.001

Maxwell, R. M., Chow, F. K., & Kollet, S. J. (2007). The groundwater–land-surface–atmosphere connection: Soil moisture effects on the atmospheric boundary layer in fully-coupled simulations. *Advances in Water Resources*, *30*(12), 2447–2466. https://doi.org/10.1016/j.advwatres.2007.05.018

Maxwell, R. M., & Condon, L. E. (2016). Connections between groundwater flow and transpiration partitioning. *Science*, *353*(6297), 377–380. https://doi.org/10.1126/science.aaf7891

Maxwell, R. M., & Miller, N. L. (2005). Development of a coupled land surface and groundwater model. *Journal of Hydrometeorology*, *6*(3), 233–247. https://doi.org/10.1175/jhm422.1

Montzka, C., Bogena, H. R., Zreda, M., Monerris, A., Morrison, R., Muddu, S., & Vereecken, H. (2017). Validation of spaceborne and modelled surface soil moisture products with cosmic-ray neutron probes. *Remote Sensing*, *9*(2), 103. https://doi.org/10.3390/rs9020103

Montzka, C., Pauwels, V. R., Franssen, H.-J. H., Han, X., & Vereecken, H. (2012). Multivariate and multiscale data assimilation in terrestrial systems: A review. *Sensors*, *12*(12), 16291–16333. https://doi.org/10.3390/s121216291

Nair, A. S., & Indu, J. (2019). Improvement of land surface model simulations over India via data assimilation of satellite-based soil moisture products. *Journal of Hydrology*, *573*, 406–421.

NASA National Snow Ice Data Center Distributed Active Archive and Center, & National Snow Ice Data and Center. (2024). SMAP L3 radar/radiometer global daily 9 km EASE-grid soil moisture [Dataset]. *National Snow and Ice Data Center (NSIDC)*. https://doi.org/10.5067/7KKNQ5UURM2W

Naz, B. S., Kurtz, W., Montzka, C., Sharples, W., Goergen, K., Keune, J., et al. (2019). Improving soil moisture and runoff simulations at 3 km over Europe using land surface data assimilation. *Hydrology and Earth System Sciences*, *23*(1), 277–301. https://doi.org/10.5194/hess-23-277-2019

Nearing, G. S., Mocko, D. M., Peters-Lidard, C. D., Kumar, S. V., & Xia, Y. (2016). Benchmarking NLDAS-2 soil moisture and evapotranspiration to separate uncertainty contributions. *Journal of Hydrometeorology*, *17*(3), 745–759. https://doi.org/10.1175/jhm-d-15-0063.1

Nearing, G. S., Ruddell, B. L., Clark, M. P., Nijssen, B., & Peters-Lidard, C. (2018). Benchmarking and process diagnostics of land models. *Journal of Hydrometeorology*, *19*(11), 1835–1852. https://doi.org/10.1175/jhm-d-17-0209.1

Nerger, L. (2023). PDAF [Software]. *Zenodo*. https://doi.org/10.5281/zenodo.7861829

Nerger, L., & Hiller, W. (2013). Software for ensemble-based data assimilation systems—Implementation strategies and scalability. *Computers & Geosciences*, *55*, 110–118. https://doi.org/10.1016/j.cageo.2012.03.026

Nerger, L., Hiller, W., & Schröter, J. (2005). PDAF-the parallel data assimilation framework: Experiences with Kalman filtering. In *Use of high performance computing in meteorology* (pp. 63–83). World Scientific.

Nie, W., Kumar, S. V., Arsenault, K. R., Peters-Lidard, C. D., Mladenova, I. E., Bergaoui, K., et al. (2022). Towards effective drought monitoring in the Middle East and North Africa (MENA) region: Implications from assimilating leaf area index and soil moisture into the noah-mp land surface model for Morocco. *Hydrology and Earth System Sciences*, *26*(9), 2365–2386. https://doi.org/10.5194/hess-26-2365-2022

Niu, G.-Y., Paniconi, C., Troch, P. A., Scott, R. L., Durcik, M., Zeng, X., et al. (2014). An integrated modelling framework of catchment-scale ecohydrological processes: 1. Model description and tests over an energy-limited watershed. *Ecohydrology*, *7*(2), 427–439. https://doi.org/10.1002/eco.1362

Niu, G.-Y., Troch, P. A., Paniconi, C., Scott, R. L., Durcik, M., Zeng, X., et al. (2014). An integrated modelling framework of catchment-scale ecohydrological processes: 2. The role of water subsidy by overland flow on vegetation dynamics in a semi-arid catchment. *Ecohydrology*, *7*(2), 815–827. https://doi.org/10.1002/eco.1405

Oleson, K., Dai, Y., Bonan, B., Bosilovichm, M., Dickinson, R., Dirmeyer, P., et al. (2004). *Technical description of the community land model (CLM)* (Tech. Rep.). Boulder, Colorado: National Center for Atmospheric Research (NCAR).

Oleson, K., Niu, G.-Y., Yang, Z.-L., Lawrence, D., Thornton, P., Lawrence, P., et al. (2008). Improvements to the community land model and their impact on the hydrological cycle. *Journal of Geophysical Research: Biogeosciences*, *113*(G1). https://doi.org/10.1029/2007jg000563

O'Neill, P., Bindlish, R., Chan, S., Chaubell, J., Njoku, E., & Jackson, T. (2020). *SMAP algorithm theoretical basis document: Level 2 & 3 soil moisture (passive) data products* (Tech. Rep.). NASA Goddard Space Flight Center.

O'Neill, P. E., Chan, S., Njoku, E. G., Jackson, T., Bindlish, R., & Chaubell, J. (2021). *SMAP enhanced L3 radiometer global and polar grid daily 9 km ease-grid soil moisture, version 5, NASA national snow and ice data center distributed active archive center*. NASA National Snow and Ice Data Center Distributed Active Archive Center. https://doi.org/10.5067/4DQ54OUIJ9DL

Ott, E., Hunt, B. R., Szunyogh, I., Zimin, A. V., Kostelich, E. J., Corazza, M., et al. (2004). A local ensemble Kalman filter for atmospheric data assimilation. *Tellus A: Dynamic Meteorology and Oceanography*, *56*(5), 415–428. https://doi.org/10.3402/tellusa.v56i5.14462

Pastorello, G., Trotta, C., Canfora, E., Chu, H., Christianson, D., Cheah, Y.-W., et al. (2020). The FLUXNET2015 dataset and the ONEFlux processing pipeline for eddy covariance data. *Scientific Data*, *7*(1), 1–27. https://doi.org/10.1038/s41597-020-0534-3

Pathiraja, S., Anghileri, D., Burlando, P., Sharma, A., Marshall, L., & Moradkhani, H. (2018). Insights on the impact of systematic model errors on data assimilation performance in changing catchments. *Advances in Water Resources*, *113*, 202–222. https://doi.org/10.1016/j.advwatres.2017.12.006

Peters-Lidard, C. D., Kumar, S. V., Mocko, D. M., & Tian, Y. (2011). Estimating evapotranspiration with land data assimilation systems. *Hydrological Processes*, *25*(26), 3979–3992. https://doi.org/10.1002/hyp.8387

Pinnington, E., Quaife, T., & Black, E. (2018). Impact of remotely sensed soil moisture and precipitation on soil moisture prediction in a data assimilation system with the Jules land surface model. *Hydrology and Earth System Sciences*, *22*(4), 2575–2588. https://doi.org/10.5194/hess-22-2575-2018

Pleim, J. E., & Xiu, A. (2003). Development of a land surface model. Part ii: Data assimilation. *Journal of Applied Meteorology*, *42*(12), 1811–1822. https://doi.org/10.1175/1520-0450(2003)042<1811:doalsm>2.0.co;2

Prakash, V., & Mishra, V. (2023). Soil moisture and streamflow data assimilation for streamflow prediction in the Narmada River basin. *Journal of Hydrometeorology*, *24*(8), 1377–1392. https://doi.org/10.1175/jhm-d-21-0139.1

Quirmbach, M., Einfalt, T., & Langstädtler, G. (2012). Climate change analysis of precipitation data for north Rhine-Westphalia. *Atmospheric Research*, *109*, 1–13.

Rahman, A., Maggioni, V., Zhang, X., Houser, P., Sauer, T., & Mocko, D. M. (2022). The joint assimilation of remotely sensed leaf area index and surface soil moisture into a land surface model. *Remote Sensing*, *14*(3), 437. https://doi.org/10.3390/rs14030437

Reichle, R. H. (2008). Data assimilation methods in the earth sciences. *Advances in Water Resources*, *31*(11), 1411–1418. https://doi.org/10.1016/j.advwatres.2008.01.001

Reichle, R. H., De Lannoy, G. J., Liu, Q., Ardizzone, J. V., Colliander, A., Conaty, A., et al. (2017). Assessment of the SMAP level-4 surface and root-zone soil moisture product using in situ measurements. *Journal of Hydrometeorology*, *18*(10), 2621–2645. https://doi.org/10.1175/jhm-d-17-0063.1

Reichle, R. H., & Koster, R. D. (2004). Bias reduction in short records of satellite soil moisture. *Geophysical Research Letters*, *31*(19). https://doi.org/10.1029/2004gl020938

Reichle, R. H., McLaughlin, D. B., & Entekhabi, D. (2002). Hydrologic data assimilation with the ensemble Kalman filter. *Monthly Weather Review*, *130*(1), 103–114. https://doi.org/10.1175/1520-0493(2002)130<0103:hdawte>2.0.co;2

Rummler, T., Arnault, J., Gochis, D., & Kunstmann, H. (2019). Role of lateral terrestrial water flow on the regional water cycle in a complex terrain region: Investigation with a fully coupled model system. *Journal of Geophysical Research: Atmospheres*, *124*(2), 507–529. https://doi.org/10.1029/2018jd029004

Ryu, D., Crow, W. T., Zhan, X., & Jackson, T. J. (2009). Correcting unintended perturbation biases in hydrologic data assimilation. *Journal of Hydrometeorology*, *10*(3), 734–750. https://doi.org/10.1175/2008jhm1038.1

Sawada, Y. (2020). Do surface lateral flows matter for data assimilation of soil moisture observations into hyperresolution land models? *Hydrology and Earth System Sciences*, *24*(8), 3881–3898. https://doi.org/10.5194/hess-24-3881-2020

Schaap, M. G. (2016). Rosetta: Pedotransfer functions for estimating soil hydraulic properties [Software]. https://www.handbook60.org/rosetta/

Seneviratne, S. I., Corti, T., Davin, E. L., Hirschi, M., Jaeger, E. B., Lehner, I., et al. (2010). Investigating soil moisture–climate interactions in a changing climate: A review. *Earth-Science Reviews*, *99*(3–4), 125–161. https://doi.org/10.1016/j.earscirev.2010.02.004

Shen, C., Niu, J., & Phanikumar, M. S. (2013). Evaluating controls on coupled hydrologic and vegetation dynamics in a humid continental climate watershed using a subsurface-land surface processes model. *Water Resources Research*, *49*(5), 2552–2572. https://doi.org/10.1002/wrcr.20189

Shi, Y., Davis, K. J., Duffy, C. J., & Yu, X. (2013). Development of a coupled land surface hydrologic model and evaluation at a critical zone observatory. *Journal of Hydrometeorology*, *14*(5), 1401–1420. https://doi.org/10.1175/jhm-d-12-0145.1

Shrestha, P., Sulis, M., Masbou, M., Kollet, S., & Simmer, C. (2014). A scale-consistent terrestrial systems modeling platform based on COSMO, CLM, and Parflow. *Monthly Weather Review*, *142*(9), 3466–3483. https://doi.org/10.1175/mwr-d-14-00029.1

Smith, S., reedmaxwell, ferguson, i., FabianGasper, Engdahl, N., Condon, L., et al. (2019). ParFlow [Software]. *Zenodo*. https://doi.org/10.5281/zenodo.3555297

Su, Z., Wen, J., Dente, L., Van Der Velde, R., Wang, L., Ma, Y., et al. (2011). The Tibetan plateau observatory of plateau scale soil moisture and soil temperature (Tibet-OBS) for quantifying uncertainties in coarse resolution satellite and model products. *Hydrology and Earth System Sciences*, *15*(7), 2303–2316. https://doi.org/10.5194/hess-15-2303-2011

Sulis, M., Keune, J., Shrestha, P., Simmer, C., & Kollet, S. (2018). Quantifying the impact of subsurface-land surface physical processes on the predictive skill of subseasonal mesoscale atmospheric simulations. *Journal of Geophysical Research: Atmospheres*, *123*(17), 9131–9151. https://doi.org/10.1029/2017jd028187

Sulis, M., Williams, J. L., Shrestha, P., Diederich, M., Simmer, C., Kollet, S. J., & Maxwell, R. M. (2017). Coupling groundwater, vegetation, and atmospheric processes: A comparison of two integrated models. *Journal of Hydrometeorology*, *18*(5), 1489–1511. https://doi.org/10.1175/jhm-d-16-0159.1

Terasaki, K., & Miyoshi, T. (2024). Including the horizontal observation error correlation in the ensemble Kalman filter: Idealized experiments with NICAM-LETKF. *Monthly Weather Review*, *152*(1), 277–293. https://doi.org/10.1175/mwr-d-23-0053.1

Tian, W., Li, X., Cheng, G.-D., Wang, X.-S., & Hu, B. (2012). Coupling a groundwater model with a land surface model to improve water and energy cycle simulation. *Hydrology and Earth System Sciences*, *16*(12), 4707–4723. https://doi.org/10.5194/hess-16-4707-2012

Tian, Z., Li, Z., Liu, G., Li, B., & Ren, T. (2016). Soil water content determination with cosmic-ray neutron sensor: Correcting aboveground hydrogen effects with thermal/fast neutron ratio. *Journal of Hydrology*, *540*, 923–933. https://doi.org/10.1016/j.jhydrol.2016.07.004

Uebel, M., & Bott, A. (2018). Influence of complex terrain and anthropogenic emissions on atmospheric co2 patterns–a high-resolution numerical analysis. *Quarterly Journal of the Royal Meteorological Society*, *144*(710), 34–47. https://doi.org/10.1002/qj.3182

Ukkola, A. M., Haughton, N., De Kauwe, M. G., Abramowitz, G., & Pitman, A. J. (2017). Fluxnetlsm r package (v1. 0): A community tool for processing fluxnet data for use in land surface modelling. *Geoscientific Model Development*, *10*(9), 3379–3390. https://doi.org/10.5194/gmd-10-3379-2017

Valcke, S. (2013). The oasis3 coupler: A European climate modelling community software. *Geoscientific Model Development*, *6*(2), 373–388. https://doi.org/10.5194/gmd-6-373-2013

Van Genuchten, M. T. (1980). A closed-form equation for predicting the hydraulic conductivity of unsaturated soils. *Soil Science Society of America Journal*, *44*(5), 892–898. https://doi.org/10.2136/sssaj1980.03615995004400050002x

Wang, Z., Timlin, D., Kouznetsov, M., Fleisher, D., Li, S., Tully, K., & Reddy, V. (2020). Coupled model of surface runoff and surface-subsurface water movement. *Advances in Water Resources*, *137*, 103499. https://doi.org/10.1016/j.advwatres.2019.103499

Yang, K., Zhu, L., Chen, Y., Zhao, L., Qin, J., Lu, H., et al. (2016). Land surface model calibration through microwave data assimilation for improving soil moisture simulations. *Journal of Hydrology*, *533*, 266–276. https://doi.org/10.1016/j.jhydrol.2015.12.018

Yetbarek, E., Kumar, S., & Ojha, R. (2020). Effects of soil heterogeneity on subsurface water movement in agricultural fields: A numerical study. *Journal of Hydrology*, *590*, 125420. https://doi.org/10.1016/j.jhydrol.2020.125420

Yin, J., Zhan, X., Zheng, Y., Hain, C. R., Liu, J., & Fang, L. (2015). Optimal ensemble size of ensemble kalman filter in sequential soil moisture data assimilation. *Geophysical Research Letters*, *42*(16), 6710–6715. https://doi.org/10.1002/2015gl063366

Zacharias, S., Bogena, H., Samaniego, L., Mauder, M., Fuß, R., Pütz, T., et al. (2011). A network of terrestrial environmental observatories in Germany. *Vadose Zone Journal*, *10*(3), 955–973. https://doi.org/10.2136/vzj2010.0139

Zamani, A., Azimian, A., Heemink, A., & Solomatine, D. (2010). Non-linear wave data assimilation with an ann-type wind-wave model and Ensemble Kalman Filter (ENKF). *Applied Mathematical Modelling*, *34*(8), 1984–1999. https://doi.org/10.1016/j.apm.2009.10.013

Zhang, L., He, C., Zhang, M., & Zhu, Y. (2019). Evaluation of the smos and SMAP soil moisture products under different vegetation types against two sparse in situ networks over arid mountainous watersheds, northwest China. *Science China Earth Sciences*, *62*(4), 703–718. https://doi.org/10.1007/s11430-018-9308-9

Zhang, R., Kim, S., & Sharma, A. (2019). A comprehensive validation of the SMAP enhanced level-3 soil moisture product using ground measurements over varied climates and landscapes. *Remote Sensing of Environment*, *223*, 82–94. https://doi.org/10.1016/j.rse.2019.01.015

Zhang, Y., & Schaap, M. G. (2017). Weighted recalibration of the Rosetta pedotransfer model with improved estimates of hydraulic parameter distributions and summary statistics (Rosetta3). *Journal of Hydrology*, *547*, 39–53. https://doi.org/10.1016/j.jhydrol.2017.01.004

Zhang, Z., Arnault, J., Laux, P., Ma, N., Wei, J., Shang, S., & Kunstmann, H. (2021). Convection-permitting fully coupled wrf-hydro ensemble simulations in high mountain environment: Impact of boundary layer-and lateral flow parameterizations on land–atmosphere interactions. *Climate Dynamics*, *59*(5–6), 1–22. https://doi.org/10.1007/s00382-021-06044-9

Zhao, H., Montzka, C., Baatz, R., Vereecken, H., & Franssen, H.-J. H. (2021). The importance of subsurface processes in land surface modeling over a temperate region: An analysis with SMAP, cosmic ray neutron sensing and triple collocation analysis. *Remote Sensing*, *13*(16), 3068. https://doi.org/10.3390/rs13163068

Zhao, H., Zeng, Y., Han, X., & Su, Z. (2023). Retrieving soil physical properties by assimilating SMAP brightness temperature observations into the community land model. *Sensors*, *23*(5), 2620. https://doi.org/10.3390/s23052620

Zheng, D., Wang, X., Van Der Velde, R., Ferrazzoli, P., Wen, J., Wang, Z., et al. (2018). Impact of surface roughness, vegetation opacity and soil permittivity on l-band microwave emission and soil moisture retrieval in the third pole environment. *Remote Sensing of Environment*, *209*, 633–647. https://doi.org/10.1016/j.rse.2018.03.011

Zhou, J., Crow, W. T., Wu, Z., Dong, J., He, H., & Feng, H. (2022). Improving soil moisture assimilation efficiency via model calibration using SMAP surface soil moisture climatology information. *Remote Sensing of Environment*, *280*, 113161. https://doi.org/10.1016/j.rse.2022.113161

Zhu, X., Shao, M., Zeng, C., Jia, X., Huang, L., Zhang, Y., & Zhu, J. (2016). Application of cosmic-ray neutron sensing to monitor soil water content in an alpine meadow ecosystem on the northern Tibetan plateau. *Journal of Hydrology*, *536*, 247–254. https://doi.org/10.1016/j.jhydrol.2016.02.038

Zreda, M., Shuttleworth, W., Zeng, X., Zweck, C., Desilets, D., Franz, T., & Rosolem, R. (2012). COSMOS: The cosmic-ray soil moisture observing system. *Hydrology and Earth System Sciences*, *16*(11), 4079–4099. https://doi.org/10.5194/hess-16-4079-2012